Gravity tectonics controls on reservoir-scale sandbodies: Insights from 3D seismic geomorphology of the canyons buried in the upper slope of the Eastern Niger delta basin

Vivian O Oguadinma, Jean-Yves Reynaud, Vincent Delhaye-Prat, Tony Akpi, Scott Thackrey, Ademola Lanisa, Massimo Dall'asta

Energy Geoscience 5 (2024) 100293

Contents lists available at ScienceDirect

Energy Geoscience

journal homepage: www.keaipublishing.com/en/journals/energy-geoscience

Gravity tectonics controls on reservoir-scale sandbodies: Insights from 3D seismic geomorphology of the canyons buried in the upper slope of the Eastern Niger delta basin

Vivian O. Oguadinma [a, b, *], Jean-Yves Reynaud [a], Vincent Delhaye-Prat [b], Tony Akpi [b], Scott Thackrey [b], Ademola Lanisa [b], Massimo Dall'Asta [b]

[a] Univ. Lille, CNRS, Univ. Littoral Côte d'Opale, UMR 8187, LOG, Laboratoire d'Océanologie et de Géosciences, F 59000 Lille, France
[b] Total Energies E & P, Africa - HUB CSTJF, Avenue Larribau, 64000, Pau, France

ARTICLE INFO

Article history:
Received 17 July 2023
Received in revised form
19 December 2023
Accepted 14 February 2024

Handling Editor: Manoj Mathew

Keywords:
Geomorphology
Submarine canyon
3D seismic
Fault
Shale ridge
Reservoir
Channel

ABSTRACT

High-resolution 3D seismic data analysis was integrated with a calibrated well and biostratigraphy data to present the first overview of a buried Pleistocene canyon system on the upper slope of the eastern Niger Delta, the Galabor Canyon. Attribute maps of specific horizons allow documenting the changing morphologies and infill lithologies of two main branches of the canyon through two stages of activity separated by a reference horizon dated at 0.99 Ma based on well calibration. At the upper slope, growth faults dissect the canyon heads, the catchment of which encroaches a network of valleys incised on the outer shelf. The canyon fill is composed of muddy channels and mass-transport deposits, largely derived from the collapse of canyon walls and sand-rich bodies forming a tract sourced by shelf-edge deltas at the outlet of the incised valleys. High-density turbiditic processes likely control the distribution of sand bodies along the canyon, ranging from tributary fans on the upper slope to 6 km-wide meander belts on the middle slope. The sandy deposits accumulate in minibasins formed along the canyon path, downstream of the subsiding hanging wall of the growth faults and upstream of shale ridges that damp the flow in the canyon. These results show that canyons can be major targets for sand reservoir exploration on the upper slope of large muddy deltas.

1. Introduction

Submarine canyons are geologic features that erode the continental shelves and slopes (Daly, 1936) creating pathways for sediment routed to the deep-water environment by mass-wasting (Godwin and Prior, 1989; Normark and Carlson, 2003) and turbiditic flows (Shepard, 1981; Normark et al., 1993; Lee et al., 1996; Poulsen et al., 1998; Pratson et al., 1994; Harris and Whiteway, 2011; Jobe et al., 2011; Zhou et al., 2015). The morphology of submarine canyons is influenced by erosional and depositional processes (O'Grady et al., 2000), involving changes in the canyon profile due to tectonic or magmatic processes (e.g. Li et al., 2016). They commonly have a V-shaped cross-section close to their head, passing down-slope to a U-shape along with a decrease in erosion and onset of deposition (Daly, 1936; Lastras et al., 2009).

The knowledge of the geomorphology of submarine canyons has increased through the years (Hagen et al., 1996; Antobreh and Krastel, 2006 Lastras et al., 2007). At the small scale, channel processes are recognized (Covault et al., 2014; Paull et al., 2011). The related coarse-grained bar forms are considered potential reservoirs (Normark et al., 1993; Barrett et al., 1998; Andrea et al., 2000; Kolla et al., 2001; Mayall and Stewart, 2001; Mayall and O'Byrne, 2002; McHargue, 2001; Posamentier and Kolla, 2003). The related sandy channel complexes are expected to occur mainly on the lower slope (Abreu et al., 2003; Deptuck et al., 2003). This is why reservoir prospection generally does not target the infill of the upper canyon reaches, composed of muddy sediments collapsed

* Corresponding author. Univ. Lille, CNRS, Univ. Littoral Côte d'Opale, UMR 8187, LOG, Laboratoire d'Océanologie et de Géosciences, F 59000 Lille, France.
E-mail address: oguadinma_vivian@yahoo.com (V.O. Oguadinma).

Production and Hosting by Elsevier on behalf of KeAi

https://doi.org/10.1016/j.engeos.2024.100293

from the canyon walls. This is further obvious in the case of mud-dominated deltas as the Niger Delta.

However, Prather et al. (2012) suggested that in an "above-graded" slope such as the Niger Delta slope (i.e., where seafloor "possesses downslope high profile, and shows subtle changes in depositional gradient resulting in low-relief stepped or terraced topography"), sand deposition might take place mainly on the mid-slope. Some sand could be deposited on the upper slope but with poor preservation potential. In Prather et al. (2012), the possibility of trapping sand in the slope was not considered as the result of canyon processes but rather the occurrence of ponded basins formed in the piggyback of gravitational thrusts. Steffens et al. (2003) demonstrated that shale-based stepped slopes (e.g., Niger Delta slope) had little ponded basins. So far, no study has been carried out concerning the interplay between canyon processes and gravity tectonics to elucidate the mechanisms of sand trapping upward in the delta slope. This is the purpose of the present research.

Based on high-quality 3D seismic data and two key well logs, this article investigates the geomorphology of a Pleistocene submarine canyon (the Galabor Canyon system, GCS). The seismic-scale landforms and processes are examined using attribute maps and their evolution through time and space using 2D sections. A tentative reconstruction of the canyon formation and evolution at the upper slope is proposed, highlighting the interplay of shale tectonics and turbiditic processes in forming sandy geobodies of economic importance.

2. Geological background

The Cenozoic Niger Delta Basin is located on the West African margin in the Gulf of Guinea (Fig. 1) and is considered a classical shale tectonic province (Wu and Bally, 2000). It covers an area of approximately 140,000 km^2 with a maximum thickness of 12 km (Allen, 1965; Evamy et al., 1978; Doust and Omatsola, 1989). The delta is one of the largest regressive ad thickest deltas globally (Tuttle et al., 1999) and is situated at the southern end of the Benue Trough, which originated during the breakup of the African and South American plates in the early Cretaceous (Whiteman, 1982). The delta depocenter, located onshore, is about 12 km thick, with sediments ranging in age from Paleocene to Present (Fig. 1).

The top unit consists of up to1.5 km thick continental sands of the Benin Formation (Avbovbo, 1978; Doust and Omatsola, 1989). The Niger deltaic successions are divided into three largely diachronous lithostratigraphic units (Fig. 2). The basal up to 7 km thick Akata Formation consists of prodelta to marine shales and is overlain by up to 3.5 km thick Agbada Formation delta front of siliciclastics and interbedded turbidite sand layers. The Delta progradations encompassing those formations extend over more than 200 km.

Continuous deposition in the basin and gravitational tectonics controlled the development of three structural zones, from shallow water to deepwater areas (Fig. 3). The extensional zone, encompassing the modern delta plain and continental shelf, is characterized by normal faults that trigger deep-seated marine shale diapirism (overpressured Akata Shale Fm. usually serving as detachment level). The translational zone, corresponding to the upper and middle slope, is dominated by mobile shales and intra-slope basins (Doust and Omatsola, 1989; Morley and Guerin, 1996). The compressional zone, in the lower slope to the deep basin, is characterized by reverse faults and detachment folds (Damuth, 1994; Cohen and McClay, 1996; Connors et al., 1998; Morgan, 2004; Bilotti et al., 2005; Corredor et al., 2005).

The influence of shale tectonics on the Niger Delta slope results in shale/thrust-cored structural highs that are flanked by several mobile shale withdrawal intra-slope basins and actively interact

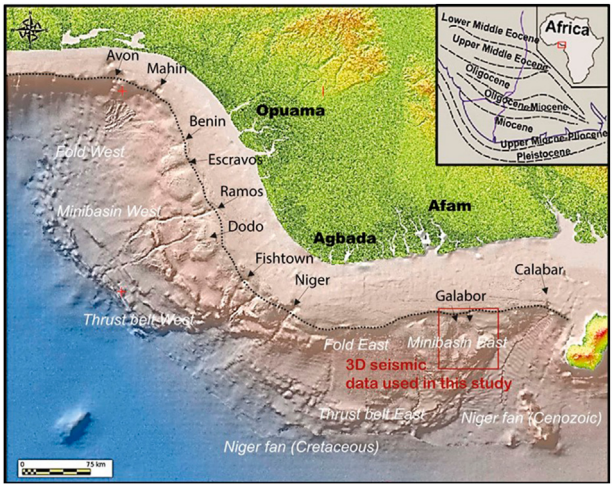

Fig. 1. Location of the study area within the Niger Delta Basin showing the present-day canyons (arrows) and approximate location of paleo-canyons (Opuama, Agbada and Afam) and main structural domains (in white). On average, the shelf edge (dotted line) is at 100 m water depth. The deep basin is at 4000 m water depth. Emerged delta plain is in green. Adapted from Rouby et al. (2011).

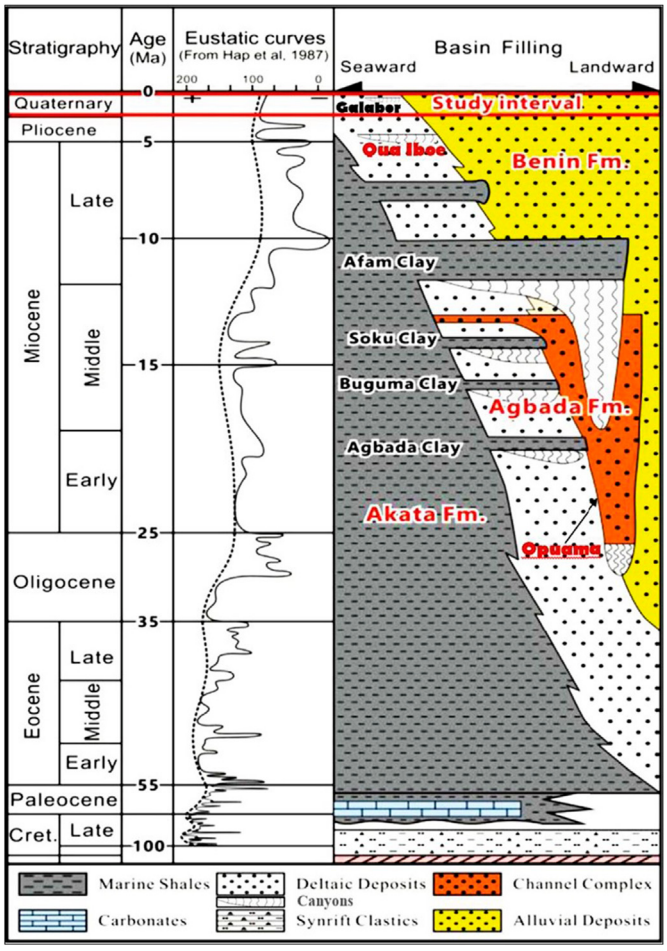

Fig. 2. Regional stratigraphic chart of the Niger Delta Basin (modified after Corredor et al., 2005). Each formation is diachronous. The present study is focused on the Quaternary part of the Agbada Formation (i.e. the canyons).

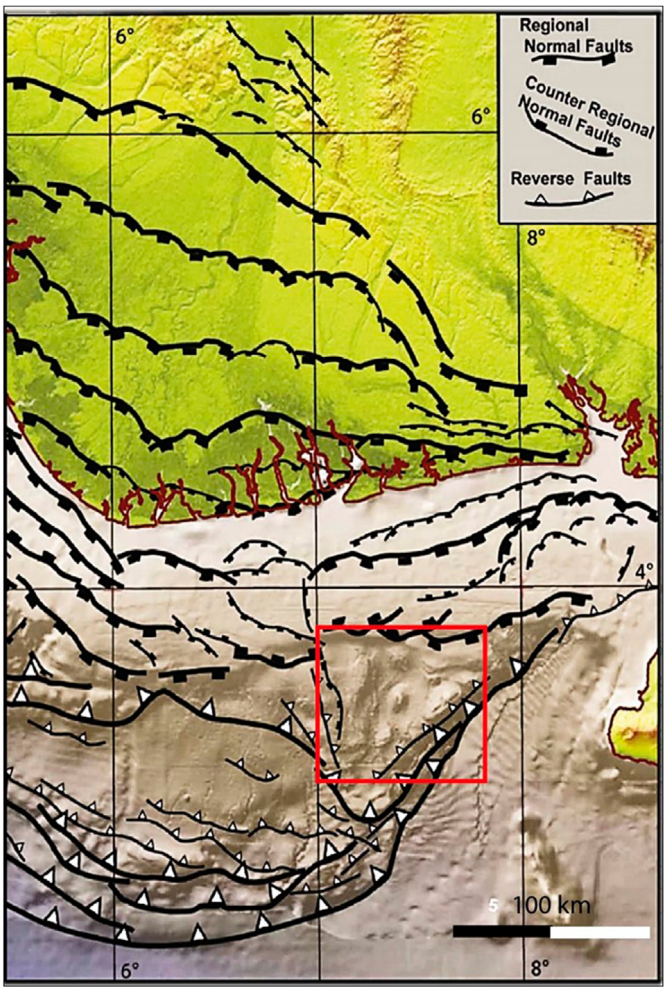

Fig. 3. Structural map of the Eastern Niger Delta. The red square is the study area at the transition between the extensional (shelf) and compressional (toe of slope) zones. After Rouby et al. (2011).

with gravity-flow sediment (Damuth, 1994; Morgan, 2004; Bilotti et al., 2005; Corredor et al., 2005; Wiener et al., 2010; Prather et al., 2012). The eastern Niger Delta slope has a dynamic equilibrium because the movements of mobile shale create constant structural highs smoothed by gravity-flow sediment that accumulates in the adjacent intraslope basins (Bakare, 2006; Prather et al., 2012; Clark and Cartwright, 2012; Chima et al., 2019). These shale structures might also control the morphology of submarine canyons and reservoir architecture (Deptuck et al., 2012; Prather et al., 2012; Jolly et al., 2016; Hansen et al., 2017; Chima et al., 2019).

Several submarine canyons of various sizes have been identified, from active to near-surface buried ones (Fig. 1), to older ones buried deeper in the Oligo-Miocene series in the Niger Delta Basin (Burke et al., 1972; Petters, 1984; Damuth, 1994; Billman, 1992). Deptuck et al. (2003, 2007) and Olabode and Adekoya (2007) explored Pleistocene canyons of the western part of the delta, where turbidity currents have been documented or inferred since the pioneering work of Burke et al. (1972). Longshore drifts caused by the southwesterly wind supply sediment to canyons entrenched close to the shoreline (e.g. Avon and Mahin canyons, Fig. 1), then evolving to gravity flows and low-density turbidites. Flow processes and the relationship to channel-belt aggradation were approached starting with 3D reflection seismics (Deptuck et al., 2007), while Abd El-Gawad et al. (2012) used a 3D numerical model to simulate turbiditic current. The latter authors concluded that seafloor topography had firm control over turbidity current dynamics. The most recent studies of the Niger Delta Pleistocene of modern canyons all focus on the western part, documenting channel facies geometries (Adeogba et al., 2005; Jimoh et al., 2018) or related fluid migration (Benjamin et al., 2015).

3. Data and methods

3.1. Seismic data and calibration

The available dataset for this study includes 4500 km^2 of 3D "high-resolution" seismic data encompassing the shelf edge and upper to middle slope in the Galabor minibasin area (Fig. 4). The seismic data set is a 3D "Pre-Stack-Time-Migration cube" with a bin spacing of 12.5 m × 12.5 m. The vertical sampling rate of the dataset is 4 ms. Considering that the dominant frequency of the data in the shallower part (about 1 s below the seabed; our reference interval for this study) is 38 Hz with an average velocity of about 1.7 km/s, the resolution is 10–12 m. The convention of the seismic data is zero-phased and in normal polarity (American standard) with an increase of impendence corresponding to a pick (positive event = black), while a decrease of impedance corresponding to a trough (negative event = red).

The seismic data are calibrated lithologically and biostratigraphically based on data of two boreholes located on the upper slope (Fig. 5; more wells are present in the study area but are not logged in the study interval). The well records provide appropriately scaled gamma-ray, density, resistivity, and sonic logs. The gamma-ray logs helped delineate lithofacies (sand and shale; Fig. 5), while the density and sonic logs are used to generate synthetic seismic traces as shown in Fig. 5 to perform a precise seismic well-tie. The latter helped evaluate the seismic response of intersected lithologies. Cuttings collected from Well-1 provide biostratigraphic information that helps to calibrate the age of the seismic record. Calcareous nannofossils biozone boundaries follow generally maximum flooding surfaces (Morley, 1996; Adeonipekun et al., 2016). The lowermost occurrence of Gephyrocapsa (Top NN19a, Calcareous Nannofossil) delineates the Middle Calabrian boundary at about 1.1 My. In addition, two main Key Surfaces (maximum flooding surfaces) were picked at the base of the Galabor Canyon's incisions, which can be correlated over most of the seismic volume. Other key surfaces have been interpreted from previous studies done on this sector of the eastern Niger Delta by Jermannaud et al. (2010) and Riboulot et al. (2012).

The sandy submarine channel deposits infilling the canyons are characterized by high to moderate seismic reflectivity and high root mean square (RMS) amplitudes on 3D maps (Posamentier and Kolla, 2003; Catuneanu, 2006). The seismic-stratigraphic analysis approach of Mitchum and Vail (1977) and the 3D geomorphology methods of Posamentier and Kolla (2003), as well as Richardson et al. (2011) were adopted. Unconformities and condensed sections (MFS) have been picked extensively following the seismic well-tie in the 3D dataset. Previously described depositional architectures in the Niger Delta include turbidite systems, hemipelagites, and mass-transport deposits (MTDs). In this study, MTDs were observed and recognized based on shear surfaces which delimit the overlying deformed and chaotic materials and the underlying, relatively continuous and undisturbed materials (Alves and Lourenço, 2010; Gamberi et al., 2011, 2015) and by the presence of rugose/irregular topographic tops (Richardson et al., 2011).

Restoration of some horizons prior to their deformation was performed using the Move™ software, namely in order to reconstruct the paleoslope dip of canyon thalwegs.

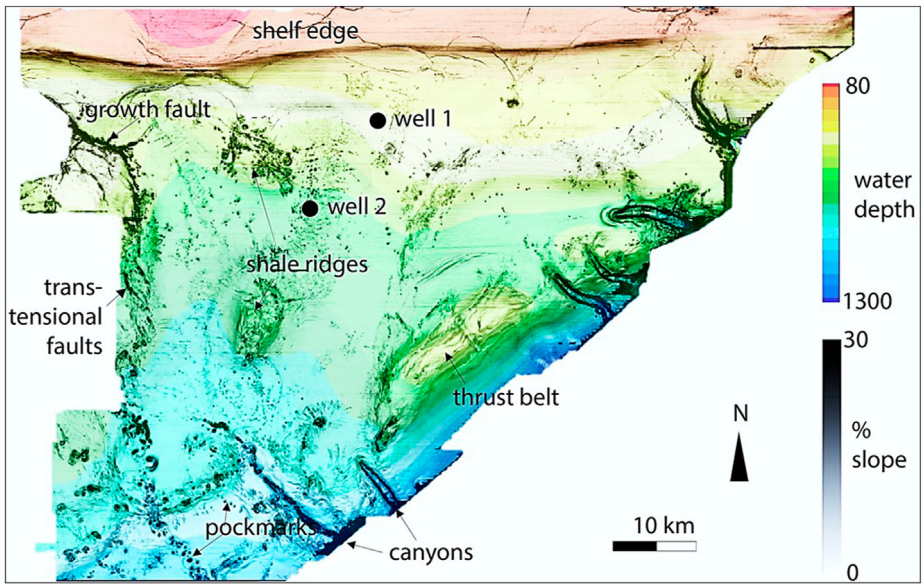

Fig. 4. Seabed bathymetry and morphology of the study area derived from coherency attribute map. The highlighted features have equivalents buried within the first 2 km of sediment in the study area.

3.2. 3D seismic geomorphology

The 3D seismic geomorphological assessment relies on attribute maps as coherency, spectral decomposition, or root means square (RMS) amplitude maps (Posamentier and Kolla, 2003; Hansen et al., 2017; Catuneanu, 2006). These maps are used to figure out the geometry and interpret the lithology of geobodies (e.g. Chopra and Marfurt, 2007; Taner et al., 1994). In this study, the RMS, spectral decomposition, and coherency attributes were applied as a routine to the 3D seismic data using Sismage™ software. The RMS attribute computes the square root of the sum of squared amplitudes over a specific geological interval of interest (called horizon) and aids in observing geometries of geobodies characterized by multiphase events as channels/complexes (Catuneanu, 2006). A 30–60 ms (two-way time, twt) window was needed to extract the characteristics/geometries of the studied geobodies (at least 2 phases picked across the targeted horizon). These values consider the seismic resolution, the sampling rate of the data and the size of the objects to be identified. The spectral decomposition and the coherency attributes maps are extracted from the picked horizons. The frequencies selected for the spectral decomposition (RGB blending) were derived from frequency analysis of the interval of interest in the 3D seismic volume based on Peyton (1998). The coherency attribute emphasized the autocorrelation of trace by trace and was mainly used to delineate structural and stratigraphic discontinuities such as faults, mobile shales, pockmarks, shelf edge delta and other geological features (Elliot, 1986, 1989). Although all the attributes mentioned above were used to explore the horizons picked in this study, the spectral decomposition maps showed better imaging and therefore were chosen to illustrate this contribution. In the next sections they are called “seismic maps” for the sake of simplicity.

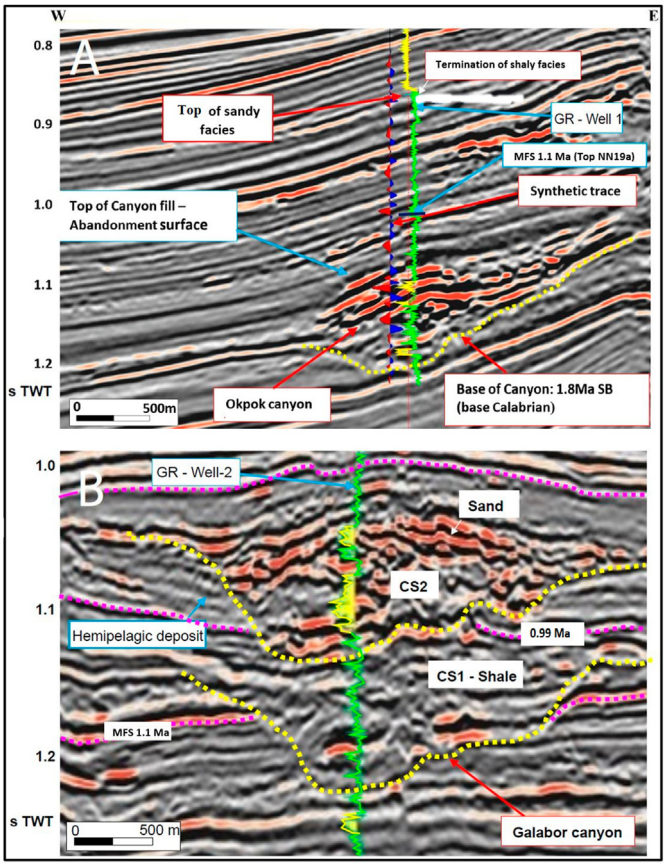

Fig. 5. Gamma-ray record (GR) of wells tied to seismic profiles showing the higher amplitude of sand (yellow) as compared to mud (green). A seismic synthetic trace is shown for well 1 down to Okpok canyon (A). This calibration is used as a template for Galabor Canyon (B). CS1 = canyon system 1 (dominantly muddy) and CS2 = canyon system 2 (dominantly sandy). Location of the two wells (Well 1 & Well 2) in Fig. 4.

4. Results

4.1. Outline

Seabed morphology reflects mainly slope processes because most of the seismic data-set is located within an upper-slope environment (Fig. 4). In the subsurface, two horizon maps are highlighted in this study (Fig. 6). Details of the geomorphologic features are provided by zooming on those horizon maps (Fig. 7). The first map, 100ms twt beneath the seabed, provides a detailed

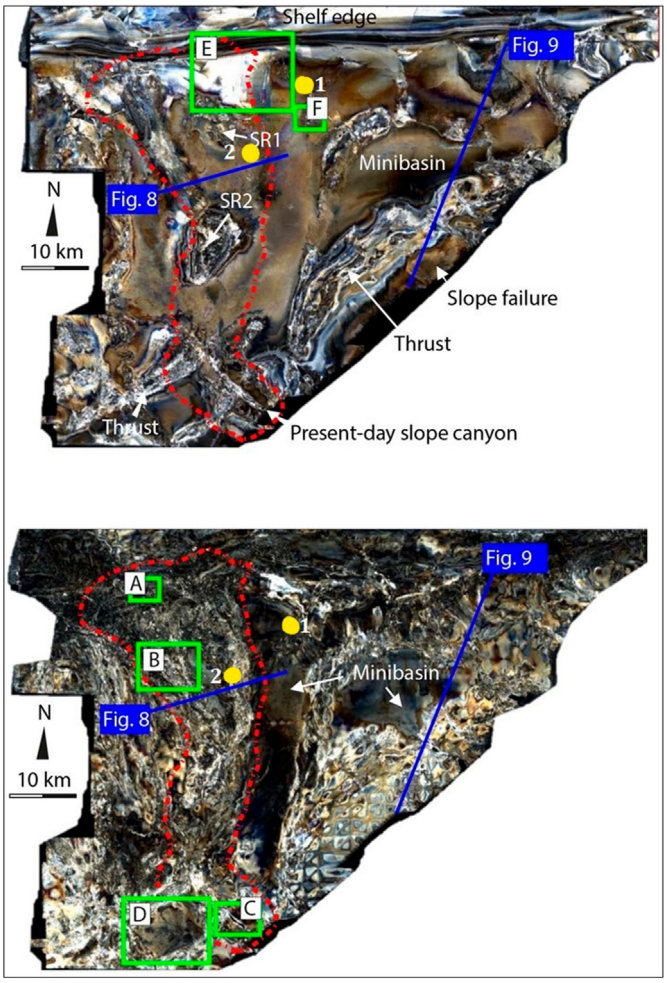

Fig. 6. Spectral decomposition maps of a horizon 100 ms twt below seabed (above) and the reference horizon within the Galabor Canyon system (bottom), about 500 ms twt below the seabed. The structural highs (shale ridges, thrusts) and lows (minibasins and canyon fairways) are well expressed near seabed and, for most of them, already marked during the canyon evolution. The dotted red line delineates the canyon area (detailed in Fig. 10). The green frames are the locations of specific features detailed in Fig. 7. The blue lines correspond to the cross sections in Figs. 8 and 9, and the yellow circles represent the locations of well 1 and 2.

image of the slope by the end of Galabor Canyon infilling. The second one, around 500ms twt beneath the seabed, is the Top Calabrian Maximum Flooding Surface, a reference marker (MFS 0.9 Ma) separating two stages of the canyon evolution, canyon systems 1 and 2 (CS1 and CS2, Fig. 8). The general stratigraphic and structural organization between the horizon maps is illustrated by large-scale seismic cross sections (Figs. 8 and 9). Isochron maps evaluate the interplay of structures on sedimentation (Fig. 10). Combined with the seismic maps, seismic profiles account for interpreting the preserved geobodies (Figs. 11 and 12). A tentative restoration of the topography of the canyon system is proposed (Fig. 13). Finally, the combined data are used for reconstructing paleogeographic maps of the canyon system (Figs. 14–16).

4.2. Seabed morphology

The shelf edge in the study area is regular and abrupt at about 180 m below sea level (Fig. 4). There are pronounced average slope values and local variations due to the presence of shale ridges. The upper slope is stepped by curvate faults (with concavity toward the slope) or en-echelon fault scarps (Fig. 4) and scattered by chaotic mounds, corresponding to the top of MTDs. The faults are the cropping part of large growth faults systems well imaged on the seismic data. The middle slope comprises shale ridges, 5–10 km wide and >1 km thick, surrounded by gullies and fault scarps (Fig. 4). The lower slope, which extends much beyond the study area, is characterized by elongated slope-parallel shale ridges, up to 20 km long and 7 km wide, that corresponds to the top of thrust folds and roughly limit the upslope extent of active canyons (Fig. 4). Pockmarks are present in the middle to lower slope, where they form elongated fields parallel to the buried canyons water escape features due to compaction or extending from their head upward in the slope (Fig. 4). Most of those elements have counterparts in the subsurface. The modern canyons in this area are initiated at the outlet of ponded minibasins at the junction between the middle and the lower slope (in about 900 m water depth, Fig. 4). The seismic profiles across these modern canyons show that their banks crosscut hemipelagic deposits, supporting the idea that they are active.

4.3. The buried canyon system

4.3.1. Keys for canyon tracing

The bulk of the deposits in the 1s twt within the studied interval is mud, as documented by the wells, forming in seismic cross sections layers of continuous reflectivity (increasing in amplitude toward the surface due to a lesser attenuation; Fig. 8). These layers are folded in wide synclines and narrow anticlines, the latter coinciding with the shale ridges at the seabed, sometimes traversed by giant pockmarks (Figs. 8 and 9, see their aspect in seismic maps in Fig. 7F). The hemipelagic deposits are interstratified with the buried canyon fill, which is dominantly composed of sand, as evidenced by well logs (Fig. 5). The canyon system is defined as such because it corresponds to a system of (mostly) erosionally-based sandy fairways (Fig. 8). In the rest of the studied seismic volume, approximately at the same depth beneath the seabed, there are other major erosional unconformities, mainly expressed atop of anticlines but these are not overlain by sand, rather by hemipelagic muds (Fig. 9). At the border of major shale ridges, these erosional unconformities clearly correspond to slope failures, up to 10 km in lateral extent and 0.4 s twt in height (e.g. the one in Figs. 9 and 6A). These unconformities might correlate with an increase in sand content in the conformable succession infilling the minibasins (Fig. 9). In that case, the sand is neither considered as a canyon fairway because it is not organized in large bodies nor bounded by an erosional unconformity. The Pleistocene Galabor Canyon system, about 70 km long and 500 ms twt thick, is buried beneath ca. 500 ms twt of hemipelagic sediments (Fig. 8). It rises downslope to the seabed to merge with the two modern canyon heads located in the SW of the study area (Fig. 6). While the sandy fairways are well imaged on seismic maps that intersect them (Fig. 6B), they still can be detected on maps extracted from the muddy seal above them, based on the numerous pockmarks that follow their route.

4.3.2. Canyon route

The Galabor Canyon system is composed of two tributary branches (east and west), each about 35 km long, that can be mapped from the reference horizon map (Fig. 6B). The reference horizon corresponds to a final stage of maximum entrenchment and subsequent infill of the canyon, and this is why it provides a good image of the two branches. These branches roughly follow the lower part of the synclines (Fig. 10 left). Below and above the reference horizon, the synclines (minibasins) also contain channels, but these are mostly unconfined (ex. Fig. 12A2). The analysis of these bodies is beyond the scope of this contribution that instead

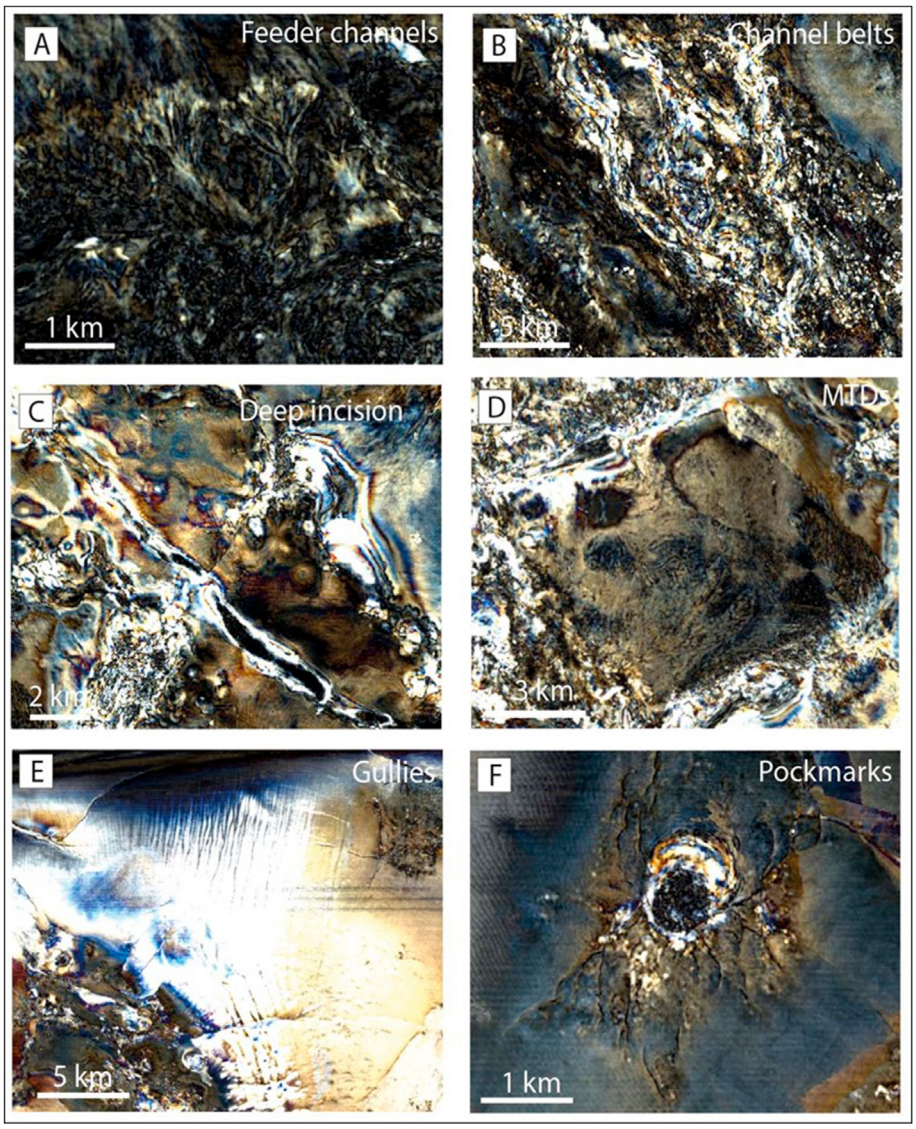

Fig. 7. Geologic features of the two reference horizons on spectral decomposition maps (from three frequency bands: red-70 Hz, green-55 Hz, blue-40 Hz): (A)Feeder channels, (B) channel belts, (C) deep incision, and (D) MTD in the reference horizon as well as (E) gullies and (F) pockmarks in the horizon 100 ms twt below seabed. See the locations in Fig. 6.

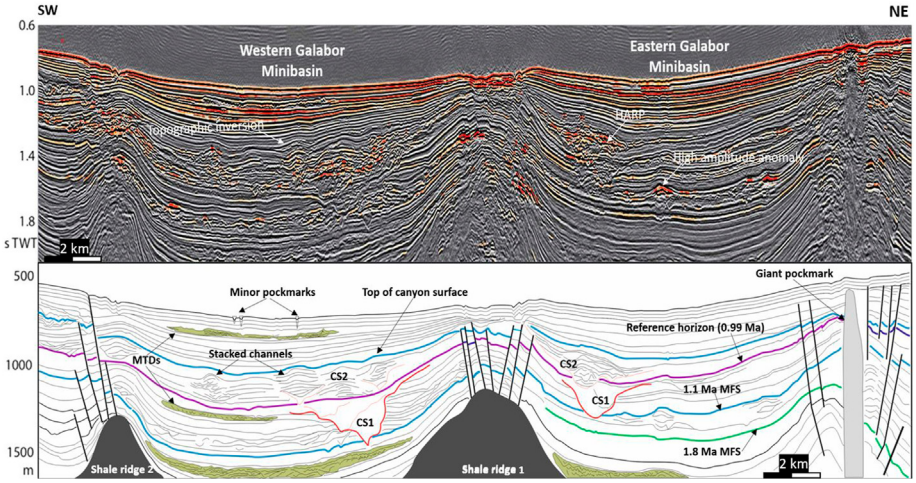

Fig. 8. Interpreted seismic cross section highlighting the main geologic features of the Galabor Canyon system on the upper slope. The purple surface aged at 0.99 Ma (tied to well 2) corresponds to an abandonment stage between two periods on canyon incision and is used as the reference horizon. The key surfaces at 1.8 Ma and 1.1 Ma are maximum flooding surfaces which are keys surfaces in the 3D seismic (Jermannaud et al., 2010).

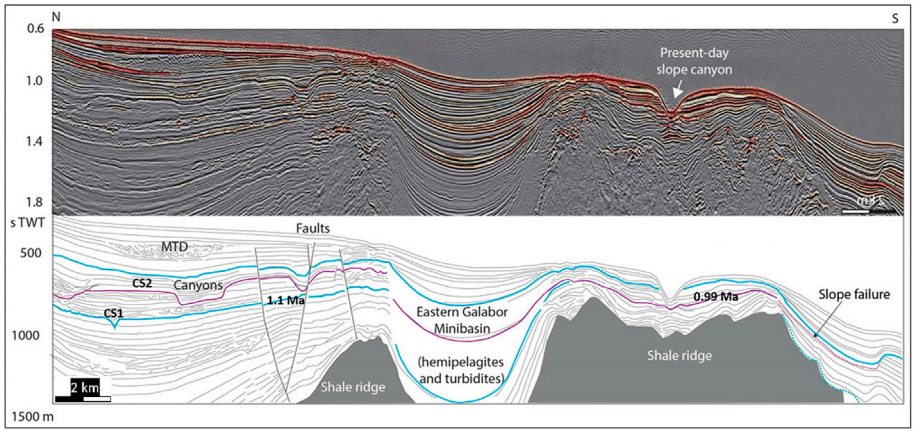

Fig. 9. Section showing the confinement of one minibasin between shale ridges. The normal faults are cogenetic with the shale ridge. Canyon systems and unconformities atop the shale ridges correlate with sandy deposits in the minibasin.

focuses on the climax cut-and-fill stage of CS1 (Fig. 8). The two canyon branches are separated by shale ridge one (SR1), which still bounds minibasins after the burial of the canyon (Fig. 8). They merge south to SR1 to form a single trunk that is further deflected by shale ridge two (SR2) and finally crosscuts the SW tip of the elongated shale ridge that limits the middle and lower slope (Figs. 6 and 10).

4.3.3. Shape of incision

The canyon branches are mostly linear, except for their upper reaches, which are composed of the coalescence of smaller tributaries. This is especially the case for the upper reaches of the western canyon branch, which comprises 3 main tributaries, 0.5–2 km wide (Fig. 10, in the A2 section). Dimensions of the canyon main incisions are measured from several cross-sectional profiles and compared with thalweg parameters in the related areas, such as slope gradient and sinuosity (Figs. 10 and 12; Table 1). Due to the presence of stepped terraces, the canyon width increases from the bottom upwards, and also from its head downslope, from about 1 km up to 5 km (Fig. 12). The canyon depth increases along with its width, from 150 ms twt (A2 in Fig. 12) to 250 ms twt (D3 in Fig. 12). These are estimates based on the elevation of canyon walls that are onlapped by a continuous succession of strata. This is not necessarily a synchronous increase downslope. For instance, in the examples given, the maximum depth in D3 is that achieved at maximum incision during CS2, while in A2, it is the maximum incision achieved during CS1. The canyon floor has a V shape, passing to a U shape in specific areas that are also where the aspect ratio (W/T) is maximum for both CS1 and CS2 (Table 1). These sections are in the vicinity of shale ridges (compare Figs. 10 and 12), as shown by the more pronounced deformation of the basement hemipelagic strata (Fig. 12). Canyon necks, which are areas of abrupt narrowing and entrenchment of the canyon, are also found to occur where the canyon crosscuts an elongated shale ridge. The basement beneath canyon necks is affected by faulting and shrinking (Fig. 11A and 12D1 & D2).

4.3.4. Growth faults

Three major growth faults were at play in controlling canyon head morphology and location in the studied area (F1 to F3 in Fig. 15). Descriptions of the base of the canyon and reference horizon were compared to show the timing of fault activity as faults are sealed at various elevations depending on the age of their last play. F1 is coeval to CS1 east of the shale ridges, while F2 and F3 are coeval to CS2. F1 and F2 are connected to two different tributaries of the eastern canyon branch, while F3 is connected to the western branch. The throw of F1 and F2 are 330 m and 150 m, respectively. Other faults of lesser throw (F4 and F5) are downslope across the canyon route.

4.4. Canyon-fill deposits

4.4.1. Appraisal of sandiness

The sand bodies at the reservoir scale are grouped in larger-scale depositional geometries that can be described regarding their planform geomorphology from seismic maps that follow time horizons (Table 2, Figs. 6, 7, 10 and 14). The spectral decomposition map of the reference horizon shows well the route and pattern of sand preserved in the system, as this horizon is the one where the most contrast between the canyon fill and the surrounding interfluve deposits occurs (Fig. 8). The sand content increases with reflectivity (i.e. seismic amplitude: lighter tones in Figs. 6, 7, 10 and 14). The chaotic structure of some deposits, including the occurrence of steep surfaces, can also generate bright spots on seismic maps, the interpretation of which must then take into account the information collected from seismic cross sections (e.g. they are more numerous at the deformed top of shale ridges). The sand accumulated over >100 ms twt in the seismic volume is commonly composed of discontinuous and high amplitude packages of reflectors (HARs, Figs. 11 and 12), the stratigraphic organization of which compares with the geomorphology of inset bodies in seismic maps.

4.4.2. Channelized tributary fans

The upper slope comprises several tributary feeder channels that route and concentrate the sand toward the lower part of the canyon. They form fan-shaped sand sheets in the canyon head, the width of which decreases toward the canyon trunk (Fig. 10A1). Conversely, the seismic amplitude in maps of these deposits decreases upward until they fringe out in the mud of the canyon head (compare thickness in A1 and B1 in Fig. 11). This indicates that at the apex of the sand sheets, the elementary sand bodies are relatively thinner than the imaged horizon (so, a few meters). In plane view, the elementary bodies form commonly rhombic bars a few hundred meters wide, bounded by small channels. These bodies merge to form a frondescent network (Fig. 7A). In cross sections, these sand bodies are aggrading in flat-bottom units up to 150 ms twt thick, with high amplitude reflections (HARs, Fig. 11A1 and B1). They are surrounded or traversed by a series of downdip parallel gullies, about 700 m in wavelength (Fig. 7E). These gullies, which

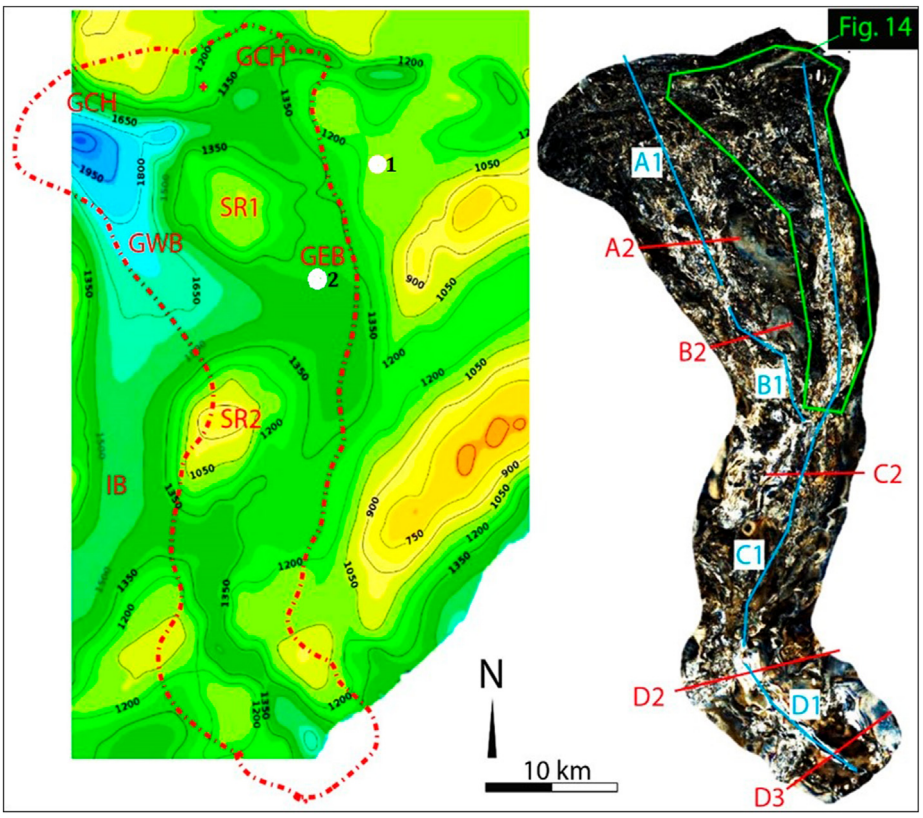

Fig. 10. Left: Isochron map of the reference horizon. The highs correspond to shale ridges, the lows to canyon fairways and minibasins. GCH: Galabor Canyon head. GWB: Galabor Western branch. GEB: Galabor Eastern branch. IB: Intraslope Basin. SR1: Shale ridge 1. SR2: Shale ridge 2. The dotted red line corresponds to the extent of the seismic map displayed to the right. Right: crop of the spectral decomposition map of the reference horizon across and around the Galabor Canyon fairways. The channel belts, dominantly composed of sand, are displayed in white, while the rest of the horizon, dominated by mud, is displayed in dark colours. Locations of seismic sections in Figs. 11 and 12 are indicated in blue and red, respectively. The white circles on the isochron map represent the locations of wells 1 and 2.

are also found outside the canyon system, extend about 20 km off the shelf-edge and are oriented toward the axis of minibasins that lie between shale ridges (Fig. 6). The feeder channels tributary fans progressively transform downslope into channel belts (Fig. 14).

4.4.3. Large channel belts

The sand in the middle slope is dominantly trapped in large braided to meander channel bars that infill the largest and deepest canyon sections. The largest meandering channel belt is formed by the end of CS1 in the eastern canyon branch (Figs. 10 and 14). In the reference horizon seismic map, the individual channels, up to 500 m wide, amalgamate to form channel belts up to 3 km wide (Fig. 7B and 14, and Table 2). The high seismic amplitude in this horizon suggests that the thickness of sand in the meander bars exceeds 10 ms twt. In cross-sections, these channel belts build up to 300 ms twt sandy facies with HARs (Fig. 11), either isolated in a muddy pile or amalgamated (Fig. 12). Where their thickness is maximum, they commonly show a cut-and-fill pattern (e.g. Baztan et al., 2005), with channel incisions up to 100 ms twt (Fig. 12D3). The channels in these sand-dominated belts are commonly plugged by mud, which makes them easy to follow on the seismic maps and to evaluate their sinuosity (ranging from 1.1 to >1.5; Tables 1 and 2) and evolution (Fig. 14). The lowest part of CS1 also contains large sinuous channel cut-and-fill structures (Fig. 12), without clear lateral accretion of channel bars, and the channels here have an overall lesser sinuosity.

4.4.4. Muddy MTDs

MTDs are up to 7 km in lateral extent and 100 m high. They are found either on the muddy slopes of the shale ridges, extending down to the center of minibasins (Fig. 8); or within the canyon fills (Fig. 12). On seismic maps, they are easily recognized from their lobate shape and the deformation features at their top (Fig. 7D). On cross sections, they have a pattern of discontinuous low to middle amplitude reflections and a conformable to erosional base (Fig. 9) and the irregular overall convex top surface (Fig. 11). Seismic amplitude of MTDs is relatively low in cross-sections, suggesting a homogenous, mostly muddy material, but can be high locally in seismic maps due to the roughness of their top surface. In the canyon fills, they are commonly intercalated with muddy channels within overall cut-and-fill units (Fig. 12).

5. Discussion

5.1. Restoring the Galabor Canyon profile

The canyon morphology is based on the restoration of the initial geometry of CS2 by flattening the Mid-Calabrian horizon along a slope fitted to the modern average slope of the seabed in the study area (Fig. 13). The original depositional canyon system thalweg dip was estimated by executing a 2D structural restoration of an axial seismic profile along the canyon. This was achieved using depth converted seismic data, which was analyzed and restored using the MOVE™ structural analysis tool. The workflow for this restoration involved firstly remapping the faults along the seismic line to achieve zero displacements at the canyon thalweg seismic marker (Fig. 13a). The structurally restored line was stripped back to the thalweg and decompacted using standard values based on the

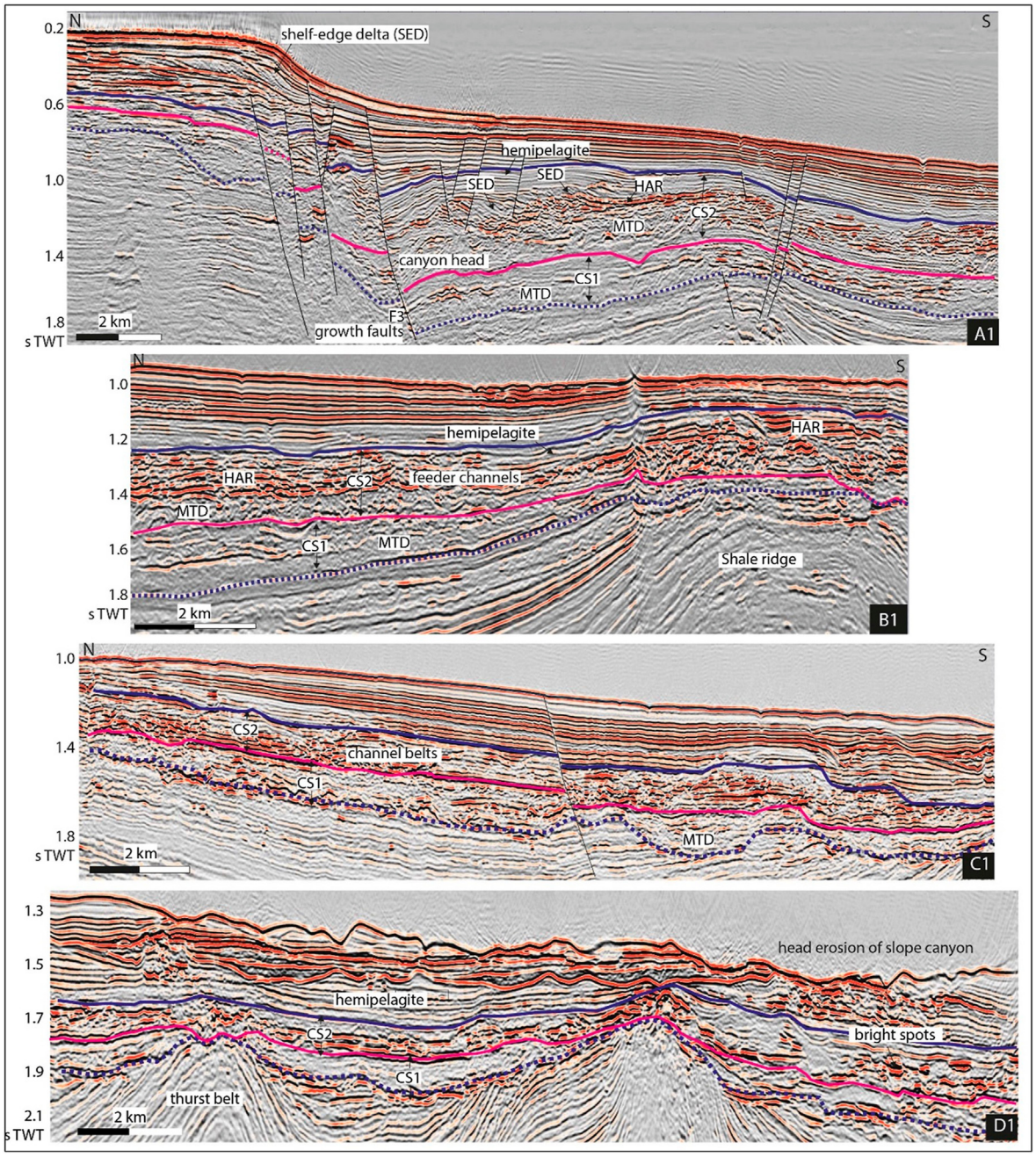

Fig. 11. Strike sections of the western branch of the Galabor Canyon in the upper and middle slope (see Fig. 10 for location). Dotted and plain blue lines mark the base and top of the canyon, respectively. The purple line marks the reference horizon. The canyon head, hosting sandy channels (high amplitude package reflectors - HARs), is indented in the shelf edge, where it connects to shelf-edge deltas (A1). The canyon section is condensed, thinner and sandier, whereas the canyon crosscuts shale ridges (B1, D). Otherwise, the canyon fill is isopachous, with little change downslope (C).

expected bulk stratigraphy. Based on the final restoration and bearing in mind the uncertainties, it can be suggested that the canyon thalweg had an approximate dip of ~0.4° to the south. This value is similar to Amazon Canyon, Mahin and Avon Canyons in the Niger Delta Basin (Hansen et al., 2017). It can be concluded that the trapping of sand in the upper slope in the Galabor Canyon is not owed to a primary geomorphic control.

5.2. Source and transport of sand

On the Niger Delta slope, as in many other margins, the hollows left behind by slope failures are suspected to be the origin of canyons (Lee et al., 2007; Shipp et al., 2011). The buried Galabor Canyon heads are mostly bounded upslope by curvate growth faults located at the shelf edge that likely created steep indents in the upper slope similar to slope failures (A1 in Fig. 11). The hanging wall of those faults comprise the toe of detached shelf-edge deltas. These shelf-edge deltas are locally preserved above MTDs, suggesting that the growth fault was already active and that the deltas prograded in the canyon catchment. The bottom sets of the delta pass downslope to the HARs and sand sheets formed by the tributary fans. Such a relationship between growth faults and the catchment of canyon

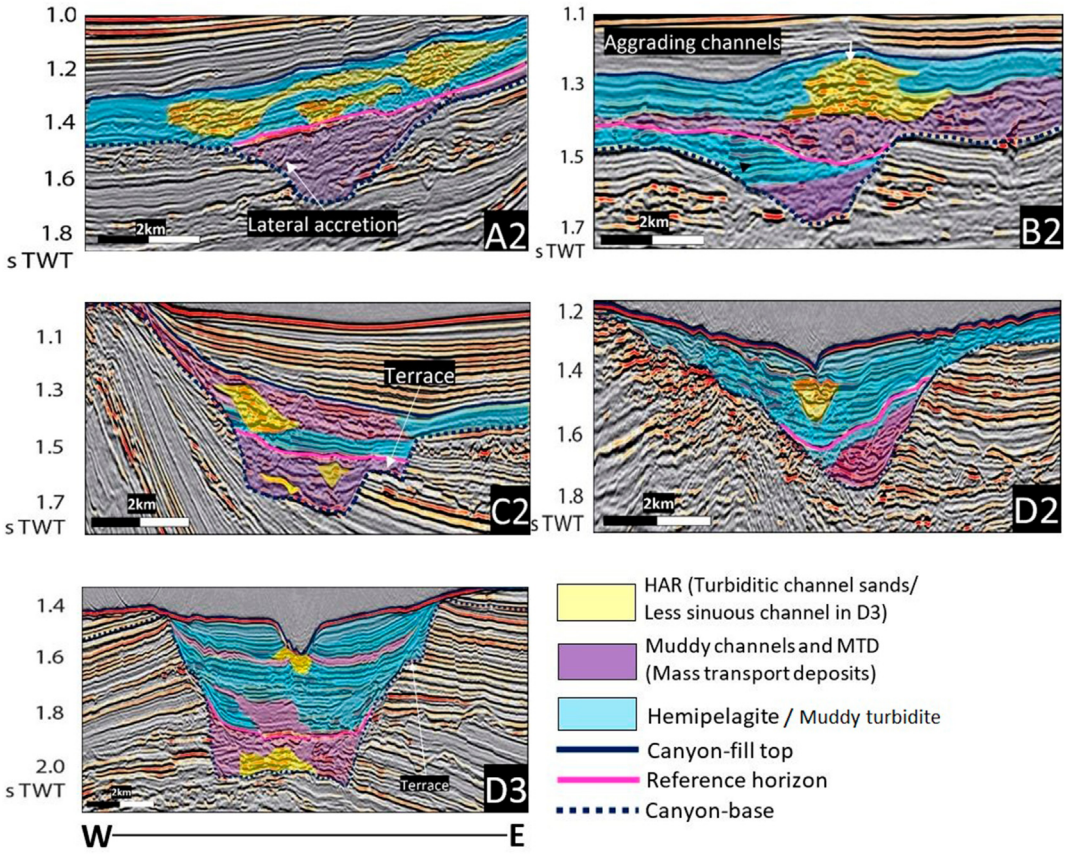

Fig. 12. Cross sections of the western branch of the Galabor Canyon (see Fig. 10 for location). The reference horizon separates the lower (CS1) and upper (CS2) units.

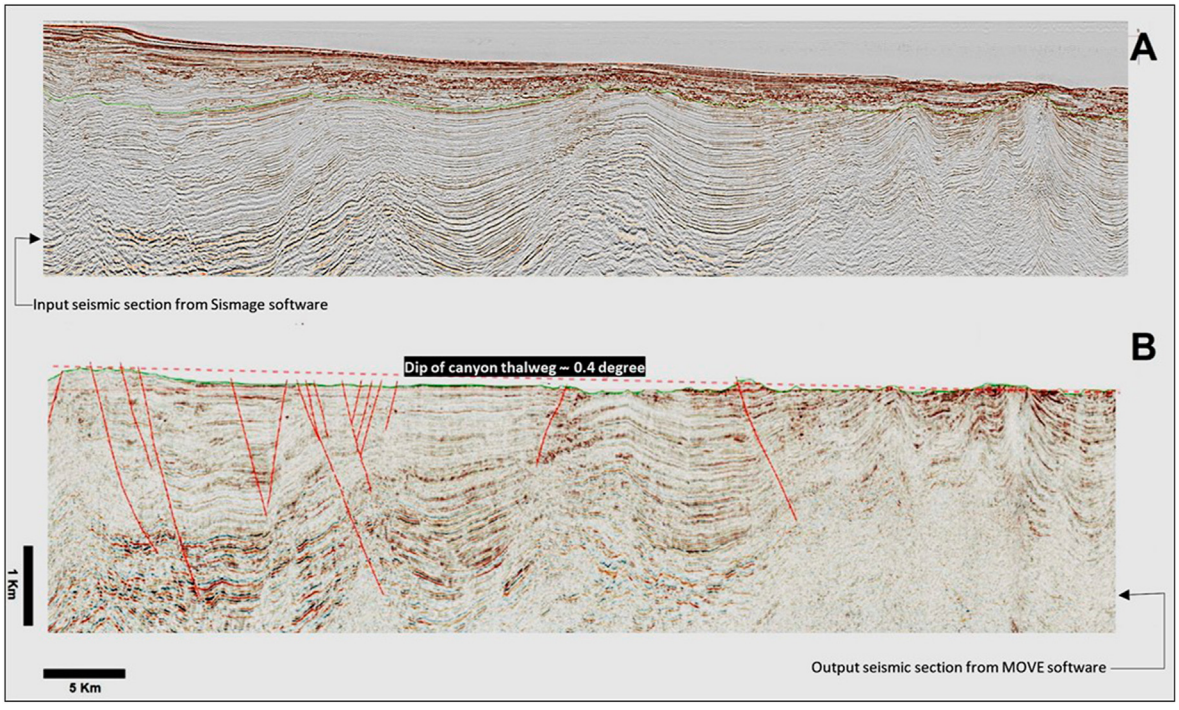

Fig. 13. Composite seismic section along the thalweg of the Galabor Canyon (blue profile in Fig. 10), restored at the canyon thalweg from (A) fault throw and (B) folding and compaction.

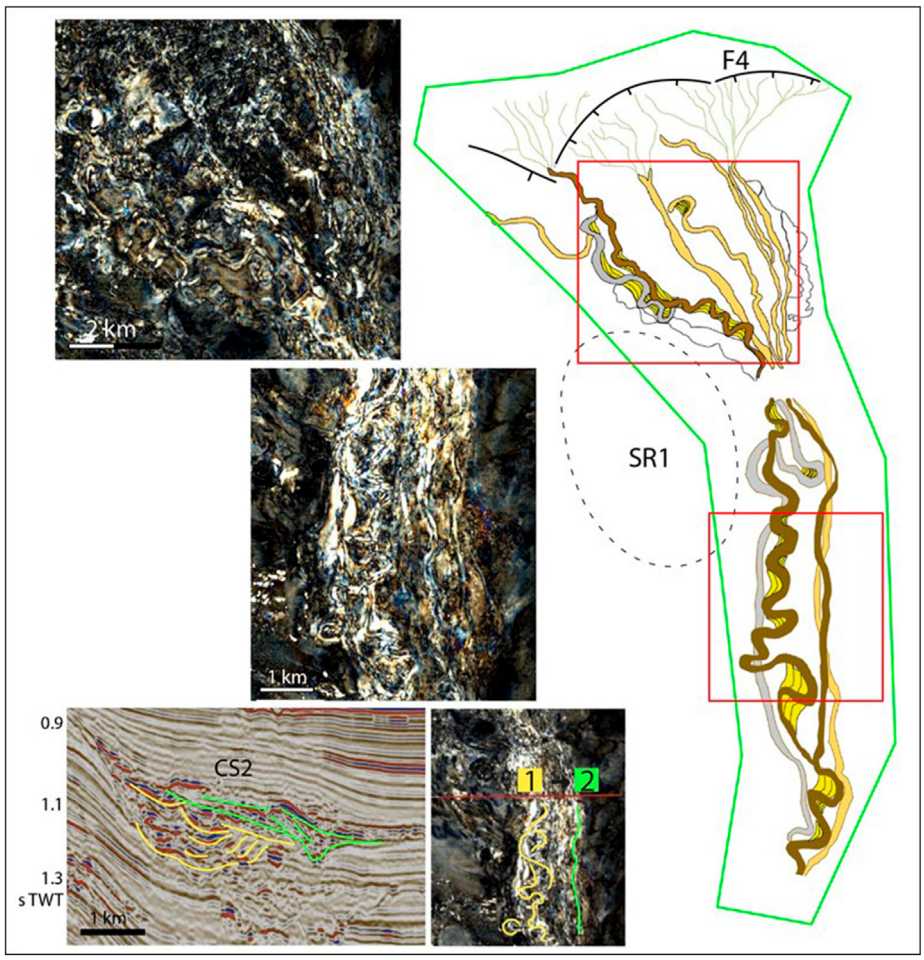

Fig. 14. Channel belts in CS2 within the eastern branch of the Galabor Canyon. The left images are closeups of the red frames. The drawing on the right (green frame located in Fig. 10) interprets the eastward shift and change in sinuosity of the channels in time. SR1: shale ridge 1. F4: fault (see Fig. 15).

heads has already been noted by Anomneze et al. (2020). Although the investigated area is restricted to a small part of the outer shelf, there might be a connection between the shelf-edge deltas and incised valleys of the outer shelf that might have supplied the sand to the system during sea-level falls (Fig. 6A).

The gently, tangential offlapping clinoforms of the shelf-edge deltas suggest a relatively low energy mechanism of dispersal of the sand, which contrasts with the gullies and bars preserved in the sand sheets built up immediately downstream in the canyon head. The bottom of the fault cliffs at the head of the sand sheets would likely be the location of hydraulic jumps, the cause of an abrupt increase in flow energy and erosion as suggested by observation in modern canyons heads (e.g. Guiastrennec-Faugas et al., 2021) and integrated in field-based facies models (Mutti et al., 2003). In the Levant basin of the Mediterranean, the rise of growth faults is observed to trigger cyclic hydraulic jumps flows (Maselli et al., 2021). Erosional events (gullies) would alternate with depositional ones (bars) through an overall by-pass-dominated system. This is consistent with the downslope transfer of most of the sand to the channel belts.

The sandy nature of the meander channel bars along the system (about 50 km observed in length) and the scarcity of sand in other geobodies shows that only a minor part of the sand load may be spilled over the channel banks and that the flow remained concentrated, confined within the channels, promoting their fast migration. The numerous muddy channel plugs that help to delineate the migration steps indicate that although lateral accretion is dominant, avulsion is a common process within the channel belt (Fig. 14). The continuous erosive character (large inertia) of the flows downslope is further supported by their overscouring in the neck areas of the canyon, as well as their maintenance at present-day low in the slope (Fig. 7C). Bottom flows would locally compete with landsliding in the process of canyon erosion, the latter being evidenced by the abundance of MTDs in the canyon fairways (Damuth and Flood, 1983; Gardner et al., 2003; Pickering et al., 1986; Posamentier and Kolla, 2003), especially in CS1.

This interpretation of the sourcing of sand in the canyon system emphasizes the control of faulting; the sand stock is already available. However, the sub-continuous activity of flows necessary for building up so large channel belts discards the idea that sand should be remobilized during faulting events only. A connection with rivers would have favoured hyperpycnal flows to form during river floods (Twichell and Roberts, 1992; Mulder and Alexander, 2001; Petter and Steel, 2006; Lastras et al., 2009; Bourget et al., 2010; Mulder and Chapron, 2011; Zhou et al., 2020). Such river connection makes most sand-bearing canyons active during sea-level lowstands.

The dominant meandering pattern of the large channels in the channel belts is common in other systems connected to high-suspension load river mouths (see examples in Deptuck and Sylvester, 2018). A large meandering channel system similar to the CS2 is also described in the western Niger Delta Pleistocene

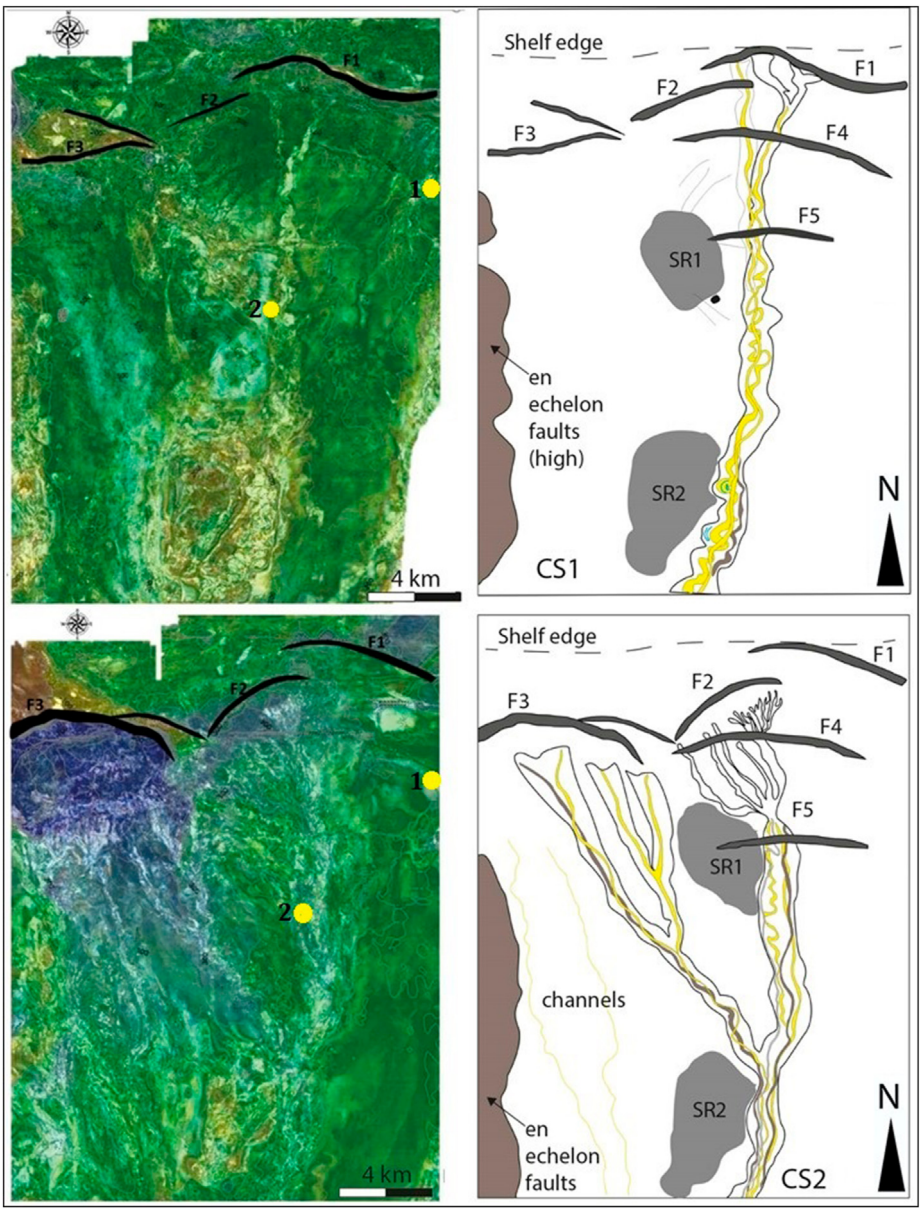

Fig. 15. Left: spectral decomposition maps of the canyon base (top) and reference horizon (bottom). Right: geomorphologic interpretation. The apparent thickness of the faults is due to the map projection. The yellow circles represent the locations of wells 1 and 2 on the spectral map.

Benin-major canyon by Deptuck et al. (2007). Implicitly, all those sand-rich canyon cuts and fills correspond to lowstand systems tracts, as demonstrated in many other case studies (e.g. Petters, 1984; Mann et al., 1992; Antobreh and Krastel, 2006; Babonneau et al., 2002). Close to the study area, the base of the Okpok canyon (name first mentioned in this manuscript) was also related to a major sea-level fall event (MIS 58; Jermannaud et al., 2010).

5.4. Tectonic control of sand trapping

Although the seismic cross sections suggest that most of the deformation (folds, namely) is post-depositional, there are numerous tiny sediment wedges in the stratigraphic pile. The fact that the canyon fairways are lying within the synclines demonstrates that their topography was already there at the time of the onset of CS1 for routing the sediment downslope. Continued deformation led to the entrenchment of the canyon across elongated shale ridge and the formation of canyon necks (canyon antecedence) with locally sharp bents, as is common in actively deforming slopes (Laursen and Normark, 2002).

A striking feature of the canyon shape in the cross-section is the flat (U-shape) bottom in C2 and D3 (Fig. 12). These are areas tilted (toward the east for C2, toward the slope for D3) due to the uplift of nearby shale ridges. At maximum incision of CS1, the tilts must have deflected the flow laterally so that this levelling should be acquired. Another consequence of this synsedimentary deformation is decreased channel sinuosity within the laterally deflected channel belts east of SR1 (Fig. 14; Table 1D2 and D3). This suggests that in this area, the overall slope gradient of the channels increased in the meantime (Table 1D2). The succession of narrow V-shaped and wide U-shaped sections along the canyon, in contrast with the Jobe et al. (2011) model, would not be a criterion of equilibrium to the base level. They would rather be a tectonic control. The V-shape sections with an irregular bottom correspond

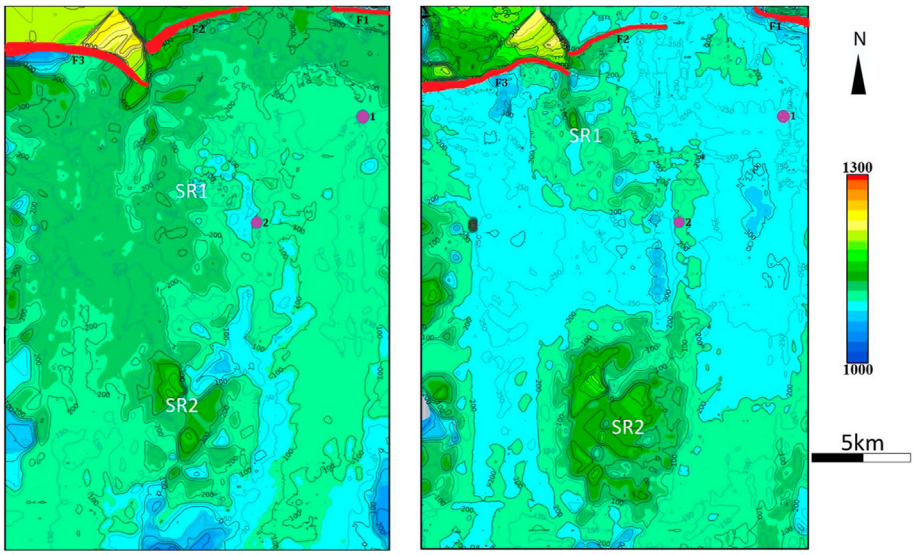

Fig. 16. Isopach maps of CS1 (left) and CS2 (right). The depocenters correspond to areas of canyon fairways and minibasins. SR1: Shale ridge 1. SR2: Shale ridge 2. See Fig. 10 for location.

Table 1
Geomorphologic parameters of the cross sections at intervals along the canyon system.

Canyon profiles cross-section profile	Thickness (m)	Average thickness (T) (m)	Width (W) (m)	Aspect Ratio (W/T)	Thickness (T) (m)	Width (W) (m)	Aspect ratio (W/T)	Average slope (°)	Sinuosity of canyon thalweg
	Entire canyon system (CS)	Canyon system One (1)	Canyon system One (1)		Canyon system Two (2)	Canyon system Two (2)			
A2	475	175	1500	9	300	5500	18	5	1.2
B2	325	175	1200	7	150	2500	17	6	1.6
C2	325	175	2600	15	155	4000	27	3	1.1
D2	425	200	1400	7	225	2600	11	11	0.9
D3	450	225	3150	14	225	3500	16	6	0.8

Table 2
Geomorphic elements of deposits in the Galabor Canyon system.

Niger Delta slope	Slope gradient (Maximum) (°)	System area size	Large-scale geometry lateral extent	Connectivity
Upper slope	5	Feeder channels 5–10 km wide	Triangular sand-sheet 1–2 km	Medium
Upper - Middle slope	3	Channel belts 6 km wide 300 m thick >45 km long	Bars: Braided (SI = 1.2) to meander (SI:1.6). Levees 3–5 km Each channel up to: 400 m wide 50 m thick	High
Middle slope: Lower part of the canyon	11	Low sinuous channels	800 m Wide 20 m thick	Unknown

to canyon shrinking across active compression structures (Fig. 11D1 and Fig. 12D2).

The deformation increments are difficult to address based on the wedging of the hemipelagites in the synclines but more easily based on the relationships between growth faults activity and accommodation. The major growth faults control topographic knick points of the thalweg profile and the thickening up of overlying deposits in the hanging wall compartment (Fig. 11A). Thickness maps calculated between reference horizons for CS1 and CS2 are used to evaluate accommodation (Fig. 16), assuming that the slope profile remained similar during all that time. These maps are a way to realize that growth faults mainly controlled accommodation. The activity of F3 during CS2 triggered the formation of the western canyon branch (Fig. 15), which was not active during CS1. There is also an interplay between the accommodation created by subsidence in the hanging wall of the faults and that created by uplifting the shale ridges. For example, while the throw of F2 during CS2 was lesser than that of F1 during CS1, the head of the eastern branch accommodated twice as many sediments in CS2 than in CS1 (Fig. 16). This is because the sediment routed downstream was damped its topographic barrier again and trapped in place due to the rise of shale ridge 1 during CS2. The frondescent pattern of the eastern canyon head in CS2, wider and shorter than that in CS1, expresses this localized trapping.

Similarly, CS2 in the western branch accommodated much sediment in the canyon head segment within the minibasins created along the canyon route between F3 and shale ridge 1. In the subsiding depocenters of minibasins, the size, sinuosity and amalgamation of meander bars are at maximum. This is the effect of suspension trapping, which is best exemplified in the minibasins

flanking shale ridge 1 (Fig. 9). It is also consistent with the fact that, in this area, the canyon slope decreases (as in the C2 gradient of 3 in Table 1), and correlatively deposition must increase.

The tectonic shrinking of thalwegs and tilting of the canyon wall in the vicinity of faults or shale ridges could probably result in reoccurring sliding and slumping of MTDs (Restrepo-Correa and Ojeda, 2010). The lesser amount of sand in the canyon fills as those locations question whether it was bypassed or damped upstream. The section downslope of the elongated ridge has a minor content of sandy channel belts (Fig. 12D3), which supports the latter interpretation. The damping of turbiditic currents due to ponding, reflection or constriction of the flow against topographic obstacles has been documented and modeled (e.g. Alexander and Morris, 1994; Patacci et al., 2015). This implies a turbiditic flow of the same height as that of the topographic barrier (about 100 ms twt, cf. Fig. 9). On the other hand, the large cut-and-fill architecture in MTDs argues in favour of a sub-continuous flow of large inertia that keeps the passageway open for the excess sand to be routed toward the deep basin.

5.5. Exploration significance

Analysis of the canyon head suggests, as in many other cases, that river-laden hyperpycnal flows, or gravity flows triggered by the faults at the shelf edge, would be responsible for the sand delivery to the Galabor Canyon. Abundant literature mentions turbidites as part of canyon fills (Carminatti and Scarton, 1991; Normark et al., 1993; Lamb and Davis, 2003; Posamentier and Kolla, 2003; Anderson et al., 2006; Prather, 2003), with sometimes emphasis put on their reservoir properties (Webb, 1981; Mayall and Stewart, 2001; McHargue, 2001; Mayall and O'Byrne, 2002; Gaudin et al., 2006). However, these canyon reservoirs were identified within canyon systems in the mid, lower, and abyssal plain (Prather, 2003; Carminatti and Scarton, 1991; Peres, 1993). In the present study, canyons buried in the upper to middle slope of a large, mud-rich delta proved to host large amounts of sand. Their housing, mostly muddy hemipelagic sediments, and the abrupt updip termination of the reservoir against the mud wall of the growth faults, make the canyon fills reservoirs prone to accumulate ascending hydrocarbons fluids. It should be noted that well-1, which penetrated the Okpok canyon directly underlying the Galabor Canyon, discovered gas. Beyond this, the presented results allow us to draw more specific conclusions regarding reservoir geobodies and facies.

The canyon system is not a simple casing of sand at all scales. The multistorey organization of either confined (entrenched in the canyon) or unconfined (more conformable in the fairway of the minibasins) sandbodies is indebted to base-level changes, the analysis of which goes beyond the scope of this contribution. The steppy fault activity pattern indicates the canyon system's subdivision in CS1 and CS2. However, within those systems, the cut-and-fill controls may follow either eustatic cycles or autocyclic geomorphic changes such as those common in fluvial or turbiditic systems. The terraced canyon walls, locally corresponding to minor unconformities within the multistorey canyon fill, reflect those base-level rises and falls (Fig. 12C and D). The longest-term control may be the encroachment of shelf-edge deltas onto the upper slope, likely triggering overloading and collapse.

Interestingly, the response of the initiation of the canyon as more or less continuous gravity flows in the long term (although discontinuous at the scale of high-frequency eustatic cycles) is not instantaneous trapping of sand. As observed in other canyons of the Niger Delta slope (Damuth, 1994; Deptuck et al., 2003, 2007), CS1 has more muddy channels (except for occasional intercalation of low sinuous channels), while CS2 has more sand (Fig. 12). The mud in CS1 is mixed with MTDs derived from the collapse of canyon walls where they are steep, a feature common in other large muddy slopes (as in the Amazon or Mississippi: Godwin and Prior, 1989; Normark and Carlson, 2003). These MTDs can locally be reworked through cut-and-fill by the turbiditic flows (Weber and Duakoru, 1975). This is likely the result of the long-term evolution of the canyon system toward a graded profile, allowing the upslope propagation of channel belts. The largest reservoir in the system is, therefore, at the top of the entire canyon system, where it reaches approximately 6 km in width and 300 m in thickness (Table 1), with a channel plugs 400 m wide and 50 m deep (Fig. 7B).

The pockmark pathways paving the horizons above the canyon sandy fairways suggest a connection to escaping overpressured fluids from the sandy geobodies. Pockmarks are craters formed on the seabed by fluid seeps (King and MacLean, 1970). These fluid escape structures suggest that at least part of the sandy deposit was under-compacted for a long time after deposition occurred. Despite the moderate overburdening (0.5 s twt), differential compaction between the sand and mud was significant, as suggested by the lens shape of the isolated channel belts in cross sections and some topographic inversions of channel fill (Fig. 12; Chopra and Marfurt, 2012). The high sedimentation rate (5 m/1000 yrs, as compared to 50 cm/1000 yrs on most passive margins) explains why the hemipelagic mud remains oversaturated at depth and, therefore, ductile. The shale ridges are tight folds formed by the extrusion of ductile materials, locally evolving toward diapirs traversed by giant pockmarks. These features are thought to form due to the overpressure imposed by overlying denser sediments with an high sedimentation rate and improper dehydration of formations (compaction desequilibrium mechanism, Short and Stauble, 1967). The overall permeability of the overburden thus questions the quality of the muddy seal of the turbiditic reservoir.

6. Conclusions

Analysis of attribute maps and cross-sections from 3D, high-resolution seismic data calibrated on two well logs provide new insights into the geomorphology and sedimentary infill of the Pleistocene Galabor Canyon, buried down to 2 s twt in the mud-dominated upper slope of the Eastern Niger Delta.

The area covered by the analyzed seismic volume corresponds to a network of minibasins formed between extensional faults at the shelf edge and toe thrust folds. Before that gravitational deformation, the Pleistocene Galabor Canyon encroached the shelf edge, which is now offset by the lower part of the delta slope. The summary of the results of the seismic study is as follows:

(1) The buried canyon system has two branches, merging in one minibasin due to the interplay of mud diapirs (shale ridges) that controlled the canyon route. The head of each of those branches is connected to an incised valley in the shelf by way of a growth fault. When the connection was active, the sand was supplied to the canyon during lowstands of sea level.
(2) The canyon valleys have a V-shaped section in the canyon head area or canyon necks across the shale ridges. They have a U-shaped section in unconfined areas or areas tilted by the growth of shale ridges. The V-shaped canyon segments are dominantly mud-filled by mass-transport deposits, while the U-shaped segments are dominantly sand-filled.
(3) The preserved sand bodies correspond to sand sheets bounded by erosion surfaces in the canyon catchments, forming channelized tributary fans. The tributary fans pass downslope up to 6 km wide and 300 m thick meander channel belts encased within the canyon walls. Hyperpycnal flows might have controlled sand transport and concentration through the system. Aggradation of the deposit was

larger in depocenters formed in the hanging wall of the growth faults or between rising shale ridges due to a decrease in slope gradient and damping of the flow.

(4) Two stages of canyon incision and infilling are observed, forming superimposed reservoirs separated by a continuous mud formed during the Calabrian (~0.9 Ma) maximum flooding. During the first stage, the canyon was mainly filled by muddy channels and mass-transport debris from the canyon wall collapse. Most of the sand was deposited during the second stage when diapir development was maximum. This suggests that topographic confinement favoured flow concentration and likely spillover of fine-grained deposits.

(5) A pavement of pockmarks traverses the mud seal of the sandy canyon and fills across 0.3 s twt, ascertaining the high fluid pressure and permeability in the canyon reservoir. Further, the perfect encasement of the sand and their abrupt updip termination against the shelf edge growth faults make them a potential target for hydrocarbon exploration.

CRediT authorship contribution statement

Vivian O. Oguadinma: Conceptualization, Formal analysis, Methodology, Software, Visualization, Writing – original draft, Writing – review & editing, Funding acquisition. **Jean-Yves Reynaud:** Conceptualization, Investigation, Supervision, Writing – review & editing. **Vincent Delhaye-Prat:** Conceptualization, Data curation, Supervision. **Tony Akpi:** Data curation, Resources. **Scott Thackrey:** Methodology. **Ademola Lanisa:** Writing – review & editing. **Massimo Dall'Asta:** Methodology, Software, Supervision, Writing – review & editing.

Declaration of competing interest

The authors declare the following financial interests/personal relationships which may be considered as potential competing interests: Oguadinma Vivian Onyinyechukwu reports financial support was provided by Petroleum Technology Development Fund. Oguadinma Vivian Onyinyechukwu reports financial support was provided by Society of Exploration Geophysicists. Oguadinma Vivian Onyinyechukwu, Delhaye-Prat Vincent, Akpi Tony, Thackrey Scott, Lanisa Ademola, and Dall'Asta Massimo are currently employed by Total Energies E & P, Pau, France.

Acknowledgements

This study is supported by the Petroleum Technology Development Fund, Nigeria, TotalEnergies Exploration and Production department, France, and the Society of Exploration Geophysicists. We thank TotalEnegies for providing and permitting the publishing of the subsurface data. We thank our colleagues, Kenechukwu NWAKWESI and Brendan FOURDAN, for their help on seismic data interpretation, technical issues, suggestions, and comments. We thank all the reviewers, who helped to improve the manuscript.

References

Abd El-Gawad, S.M., Pirmez, C., Cantelli, A., Minisini, D., Sylvester, Z., 2012. 3-D numerical simulation of turbidity currents in submarine canyons off the Niger Delta. Mar. Geol. 326–328, 55–66.

Abreu, V., Sullivan, M., Primez, C., Mohrig, D., 2003. Lateral accretion packages (LAPs): an important reservoir element in deep water sinuous channels. Mar. Petrol. Geol. 20, 631–648.

Adeogba, A.A., McHargue, T.R., Graham, S.A., 2005. Transient fan architecture and depositional controls from near-surface 3-D seismic data, Niger delta continental slope. AAPG Bull. 89, 627–643.

Adeonipekun, A.P., Agbalaya, A.E., Adeniyi, T., 2016. Aeropalynology of ayetoro-itele, ota southwest Nigeria: a preliminary study: 130–153. In: Oyelaran, P.A., Alabi, R.A., Adeonipekun, P.A. (Eds.), Human Palaeoecology in Africa: Essays in Honour of M. Adebisi Sowunmi. University of Ibadan Press, Ibadan, Nigeria, pp. 130–153.

Alexander, J., Morris, S., 1994. Observations on experimental, nonchannelized, high-concentration turbidity currents and variations in deposits around obstacles. J. Sediment. Res. 64, 899–909.

Allen, J.R.L., 1965. Late Quaternary Niger Delta and adjacent areas: sedimentary environments and lithofacies. AAPG Bull. 49, 547–600.

Alves, T.M., Lourenço, S.D.N., 2010. Geomorphologic features related to gravitational collapse: submarine landsliding to lateral spreading on a Late Miocene - Quaternary slope (SE Crete, eastern Mediterranean). Geomorphology 123, 13–33.

Andrea, F., Bloch, R.B., Webb, M.W., 2000. Evolution of Pleistocene Channel-Levee Systems Offshore Equatorial Guinea, West Africa. AAPG Annual Meeting Abstracts CD.

Anderson, K.S., Graham, S.A., Hubbard, S.M., 2006. Facies, architecture, and origin of a reservoir-scale sand-rich succession within submarine canyon fill; insights from Wagon Caves Rock (Paleocene), Santa Lucia Range, California, U.S.A. J. Sediment. Res. 76, 819–838.

Anomneze, D.O., Okoro, A.U., Ajaegwu, N.E., Akpunonu, E.O., Obiadi, I.I., Ahaneku, C.V., Okeke, G.C., 2020. Description and interpretation of fault-related sedimentation and controls on shelf-edge deltas: implication on sand transportation to the basin floor in parts of Eastern Niger Delta. J. Pet. Explor. Prod. Technol. 10, 1367–1388.

Antobreh, A., Krastel, S., 2006. Morphology, seismic characteristics, and development of Cap Timiris Canyon, offshore Mauritania: A newly discovered canyon preserved off a major arid climatic region. Mar. Petrol. Geol. 23, 37–59.

Avbovbo, A.A., 1978. Tertiary lithostratigraphy of Niger Delta. Bull AAPG 62, 295–300. Tulsa, Oklahoma.

Babonneau, N., Savoye, B., Cremer, M., Klein, B., 2002. Morphology and architecture of the present canyon and channel system of the Zaire deep-sea fan. Mar. Petrol. Geol. 19, 445–467.

Bakare, O., 2006. Effect Growing Structures on Stratigraphic Evolution, Channel Architecture, and Submarine Fan Distribution, Niger Delta, West Africa. Doctoral dissertation, Colorado School of Mines.

Barrett, M., Ruiter, A., Schirmer, T., Kapela, P., 1998. Deepwater Tertiary Turbidite Channel Exploration Plays, Block 14, Offshore Cabinda, Angola. AAPG International Conference and Exhibition Abstracts CD.

Baztan, J., Berné, S., Olivet, J.-L., Rabineau, M., Aslanian, D., Gaudin, M., Réhault, J.-P., Canal, M., 2005. Axial incision: The key to understanding submarine canyon evolution (in the western Gulf of Lion). Mar. Petrol. Geol. 22, 805–826.

Benjamin, U., Huuse, M., Hodgetts, D., 2015. Canyon-confined pockmarks on the western Niger Delta slope. J. Afr. Earth Sci. 107, 15–27.

Billman, H.G., 1992. Offshore stratigraphy and palaeontology of Dahomey (Benin) Embayment. NAPE Bull 70, 121–130.

Bilotti, F., Shaw, J.H., Corredor, F., 2005. Detachment fold, Niger delta. In: Shaw, J.H., Connors, C., Suppe, J. (Eds.), Seismic Interpretation of Contractional Fault Related Folds, AAPG Studies in Geology, vol. 53, pp. 103–104.

Bourget, J., Zaragosi, S., Mulder, T., Schneider, J.-L., Garlan, T., Van Toer, A., Mas, V., Ellouz-Zimmermannn, N., 2010. Hyperpycnal-fed turbidities lobe architecture and recent sedimentary processes: A case study from the Al Batha turbidite system, Oman margin. Sediment. Geol. 229, 144–159.

Burke, K.C., Dessauvagie, T.F.J., Whiteman, A.J., 1972. The geological history of the Benue valley and adjacent areas. Afri. Geol. 1, 7-2.

Carminatti, M., Scarton, J.C., 1991. An overview is the sequence stratigraphy of the Oligocene turbidite complex of the Campos Basin, offshore Brazil. In: Weimer, P., Link, M.H. (Eds.), Seismic Facies and Sedimentary Processes of Submarine Fans and Turbidite Systems. Springer-Verlag, New York, pp. 241–246.

Catuneanu, O., 2006. Principles of Sequence Stratigraphy. Elsevier.

Chima, K.I., Do Couto, D., Leroux, E., Gardin, S., Hoggmascall, N., Rabineau, M., Granjeon, D., Gorini, C., 2019. Seismic stratigraphy and depositional architecture of Neogene intraslope basins, offshore western Niger Delta. Mar. Petrol. Geol. 109, 449–468.

Chopra, S., Marfurt, K.J., 2007. Seismic Attributes for Prospect Identification and Reservoir Characterization. Abstract. In: Seismic Attributes for Prospect Identification and Reservoir Characterization. Society of Exploration Geophysicists and European Association of Geoscientists and Engineers, Tulsa, Oklahoma.

Chopra, S., Marfurt, K.J., 2012. Seismic Attributes expression of differential compaction. Lead. Edge 31, 1418–1422.

Clark, I.R., Cartwright, J.A., 2012. Interactions between coeval sedimentations and deformation from the Niger Delta deepwater fold belt. In: Prather, B.E., Deptuck, M.E., Mohrig, D., Van Hoorn, B., Wynn, R.B. (Eds.), Application of the Principles of Seismic Geomorphology to Continental-Slope and Base-Of-Slope Systems: Case Studies from Seafloor and Near-Seafloor Analogues, vol. 99. SEPM Special Publication, pp. 243–267.

Cohen, H.A., McClay, K., 1996. Sedimentation and shale tectonics of the northwestern Niger Delta front. Mar. Petrol. Geol. 13, 313–328.

Connors, C.D., Denson, D.B., Kristiansen, G., Angstadt, D.M., 1998. Compressive anticlines of the mid-outer slope, central Niger Delta. AAPG Bull. 82, 1903.

Corredor, F., Shaw, J.H., Bilotti, F., 2005. Structural styles in the deepwater fold and thrust belts of the Niger Delta. AAPG Bull. 89, 753–780.

Covault, J.A., Kostic, S., Paull, C.K., Ryan, H.F., Fildani, A., 2014. Submarine channel initiation, filling, and maintenance from seafloor geomorphology and morphodynamic modelling of cyclic steps. Sedimentology 61, 1031–1054.

Daly, R.A., 1936. Origin of submarine canyons. Am. J. Sci. 5, 401–420.
Damuth, J.E., Flood, R.D., 1983. Morphology, sedimentation processes, and growth pattern of the Amazon deep-sea fan. Geo Mar. Lett. 3, 109-117.
Damuth, J.E., 1994. Neogene gravity tectonics and depositional processes on the deep Niger Delta continental margin. Mar. Petrol. Geol. 11, 320–346.
Deptuck, M.E., Sylvester, Z., 2018. In: Micallef, A., Krastel, S., Savini, A. (Eds.), Submarine Fans and Their Channels, Levees, and Lobes, Submarine Geomorphology. Springer Geology. Springer, Cham, pp. 273–299.
Deptuck, M.E., Steffens, G.S., Barton, M., Pirmez, C., 2003. Architecture and evolution of upper fan channel belts on the Niger Delta slope and the Arabian Sea. Mar. Petrol. Geol. 20, 649–676.
Deptuck, M.E., Sylvester, Z., Pirmez, C., O'Byrne, C., 2007. Migration-aggradation history and 3-D seismic geomorphology of submarine channels in the Pleistocene Benin-major Canyon, western Niger Delta slope. Mar. Petrol. Geol. 24, 406–433.
Deptuck, M.E., Sylvester, Z., O'Byrne, C., 2012. Pleistocene seascape evolution above a "simple" stepped slope-western Niger Delta. In: Prather, B.E., Deptuck, M.E., Mohrig, D., Van Hoorn, B., Wynn, R.B. (Eds.), Application of the Principles of Seismic Geomorphology to Continental-Slope and Base-Of-Slope Systems: Case Studies from Seafloor and Near-Seafloor Analogues, vol. 99. SEPM Spec. Pub., pp. 199–222
Doust, H., Omatsola, E., 1989. Niger Delta. AAPG Bull. 48, 201–238.
Elliot, T., 1986. Deltas. In: Reading, H.G. (Ed.), Sedimentary Environments and Facies. Blackwell, Oxford, pp. 113–154.
Elliot, T., 1989. Deltaic systems and their contribution to an understanding of basin-fill successions. In: Whateley, M.K.G., Pickering, K.T. (Eds.), Deltas: Sites and Traps for Fossil Fuels, vol. 41. Geol.Soc. Spec. Publ., pp. 3–10
Evamy, B.D., Haremboure, J., Kamerling, P., Knaap, W.A., Molloy, F.A., Rowlands, P.H., 1978. Hydrocarbon habitat of Tertiary Niger Delta. AAPG Bull. 62, 1–39.
Gamberi, F., Rovere, M., Marani, M., 2011. Mass-transport complex evolution in a tectonically active margin (Gioia basin, Southeastern Tyrrhenian Sea). Mar. Geol. 279, 98–110.
Gamberi, F., Rovere, M., Marani, M.P., Dykstra, M., 2015. Modern deep-sea fan facies development along a tectonically active margin. Geosphere 11, 307–319.
Gardner, M.H., Borer, J.M., Melick, J.J., Maravilla, N., Dechesne, M., Wagerle, R.N., 2003. Stratigraphic process-response model for submarine channels and related features from studies of Permian Brushy Canyon outcrops, West Texas. Mar. Petrol. Geol. 20, 757-787.
Gaudin, M., Berné, S., Jouanneau, J.-M., Palanques, A., Puig, P., Mulder, T., Cirac, P., Rabineau, M., Imbert, P., 2006. Massive sand beds are attributed to deposition by dense water cascades in the Bourcart canyon head, Gulf of Lions (northwestern Mediterranean Sea). Mar. Geol. 234, 111–128.
Godwin, R.H., Prior, D.B., 1989. Geometry and depositional sequence of the Mississippi Canyon, Gulf of Mexico. J. Sediment. Petrol. 59, 318–329.
Guiastrennec-Faugas, L., Gillet, H., Peakall, J., Dennielou, B., Gaillot, A., Jacinto, R.S., 2021. Initiation and evolution of knickpoints and their role in cut-and-fill processes in active submarine channels. Geology 49, 314–319.
Hagen, R.A., Vergara, H., Naar, D.F., 1996. Morphology of San Antonio submarine canyon on the central Chile forearc. Mar. Geol. 129 (3-4), 197–205.
Hansen, L., Janocko, M., Kane, I., Kneller, B., 2017. Submarine channel evolution, terrace development, and preservation of intra-channel thin-bedded turbidites: Mahin and Avon channels, offshore Nigeria. Mar. Geol. 383, 146–167.
Harris, P.T., Whiteway, T., 2011. Global distribution of large submarine canyons: Geomorphic differences between active and passive continental margins. Mar. Geol. 285, 69–86.
Jermannaud, P., Rouby, D., Robin, C., Nalpas, T., Guillocheau, F., Raillard, S., 2010. Plio-Pleistocene sequence stratigraphic architecture of the eastern Niger Delta: A record of eustasy and aridification of Africa. Mar. Petrol. Geol. 27, 810–821.
Jimoh, R.O., Tang, Y., Li, J., Awosika, L.F., Li, H., Akinnigbage, E.A., Adeleye, A.O., 2018. The architecture of the lower parts of submarine canyons on the western Nigerian continental margin. Acta Oceanol. Sin. 37, 28–40.
Jobe, Z.R., Lowe, D.R., Uchytil, S.J., 2011. Two fundamentally different types of submarine canyons along the continental margin of Equatorial Guinea. Mar. Petrol. Geol. 28, 843–860.
Jolly, B.A., Lonergan, L., Whittaker, A.C., 2016. Growth history of fault-related folds and interaction with seabed channels in the toe-thrust region of the deepwater Niger Delta. Mar. Petrol. Geol. 70, 58–76.
King, L.H., MacLean, B., 1970. Pockmarks on the Scotian Shelf. Bull. Geol. Soc. Am. 81, 3141–3148.
Kolla, V., Bourges, P., Urruty, J.M., Safa, P., 2001. Evolution of deepwater Tertiary sinuous channels offshore Angola (West Africa) and implications for reservoir architecture. AAPG Bull. 85, 1373–1405.
Lamb, S., Davis, P., 2003. Cenozoic climate change is a possible cause for the rise of the Andes. Nature 425, 792–797.
Lastras, G., Canals, M., Urgeles, R., Amblas, D., Ivanov, M., Droz, L., dennielou, B., Fabrés, J., Schoolmeester, T., Akhmetzhanov, A., Orange, D., Garcia-Garcia, A., 2007. A walk down the Cap de Creus canyon, northwestern Mediterranean Sea: Recent processes inferred from morphology and sediment bedforms. Mar. Geol. 246, 176–192.
Lastras, G., Arzola, R.G., Masson, D.G., Wynn, R.B., Huvenne, V.A.I., Hühnerbach, V., Canals, M., 2009. Geomorphology and sedimentary features in the Central Portuguese submarine canyons, Western Iberian Margin. Geomorphology 103, 310–329.
Laursen, J., Normark, W.R., 2002. Late Quaternary evolution of the San Antonio submarine canyon in the central Chile forearc (similar to 33 degrees). Mar. Geol. 188, 365–390.
Lee, G.H., Watkins, J.S., Bryant, W.R., 1996. Bryant canyon fan system: an unconfined, large river-sourced system in the Northwestern Gulf of Mexico. AAPG Bull. 80, 340–358.
Lee, H.J., Locat, J., Desgagnés, P., Parsons, J.D., McAdoo, B.G., Orange, D.L., et al., 2007. Submarine Mass Movements on Continental Margins. In: Nittrouer, C.A., Austin, J.A., Field, M.E., Kravitz, J.H., Syvitski, J.P.M., Wiberg, P.L. (Eds.), Continental Margin Sedimentation. Blackwell Publishing Ltd., Oxford, UK, pp. 213–274.
Li, W., Alves, T.M., Wu, S., Rebesco, M., Zhao, F., Mi, L., Ma, B., 2016. A giant submarine creeps zone as a precursor of large-scale slope instability offshore the Dongsha Islands (South China Sea). Earth Planet Sci. Lett. 451, 272–284.
Mann, R.G., Bryant, W.R., Rabinowitz, P.D., 1992. Seismic facies interpretation of the Northern Green canyon Area, Gulf of Mexico. In: Watkins, K.J. (Ed.), Geology and Geophysics of Continental Margins, vol. 53. AAPG Memoir, pp. 343–360.
Maselli, V., Micallef, A., Normandeau, A., Oppo, D., Iacopini, D., Green, A., Ge, Z., 2021. Active faulting controls bedform development on a deep-water fan. Geology 49, 1495–1500.
Mayall, M., O'Byrne, C., 2002. Reservoir prediction and development challenges in turbidite slope channels. Offshore Technology Conference, OTC 1429, 1–11.
Mayall, M., Stewart, I., 2001. The architecture of turbidite slope channels. The Geological Society conference proceedings, London. In: Fraser, S.I., Fraser, A.J., Johnson, H.D., Evans, A.M. (Eds.), Petroleum Geology of Deepwater Depositional Systems, Advances in Understanding 3D Architecture.
McHargue, T., 2001. Recurring stacking pattern of reservoir elements in erosional slope valleys, Niger Delta, Nigeria. In: Fraser, S.I., Fraser, A.J., Johnson, H.D., Evans, A.M. (Eds.), Petroleum Geology of Deepwater Depositional Systems, Advances in Understanding 3D Architecture. The Geological Society conference proceedings, London.
Mitchum, R.M., Vail, P.R., 1977. Seismic stratigraphy and global sea-level changes, Part 7: seismic stratigraphic interpretation. In: Payton, C.E. (Ed.), Seismic Stratigraphy: Applications to Hydrocarbon Exploration, vol. 26. AAPG Memoir, pp. 135–143.
Morgan, R., 2004. Structural controls on the positioning of submarine channels on the lower slopes of the Niger Delta. In: Davies, R.J., Cartwright, J., Stewart, S.A., Underhill, J.R., Lappin, M. (Eds.), 3D Seismic Technology: Application to the Exploration of Sedimentary Basins, vol. 29. Geological Society of London Memoir, pp. 45–51.
Morley, C.K., Guerin, G., 1996. Comparison of gravity-driven deformation styles and behaviour associated with mobile shales and salt. Tectonics 15, 1154–1170.
Morley, R.J., 1996. Biostratigraphic characterization of systems tracts in Tertiary sedimentary basins. In: Proceedings of the International Symposium on Sequence Stratigraphy in SE Asia. IPA Jakarta, pp. 49–71.
Mulder, T., Alexander, J., 2001. The physical character of subaqueous sedimentary density flows and their deposits. Sedimentology 48, 269–299.
Mulder, T., Chapron, E., 2011. Flood deposits in continental and marine environments: Character and significance. In: Zavalaca, C., Slatt, R.M. (Eds.), Sediment Transfer from Shelf to Deepwater Revisiting the Delivery System, AAPG Studies in Geology, vol. 61, pp. 1–30.
Mutti, E., Tinterri, R., Benevelli, G., Biase, D. di, Cavanna, G., 2003. Deltaic, mixed and turbidite sedimentation of ancient foreland basins. Mar. Petrol. Geol. 20, 733–755.
Normark, W.R., Carlson, P.R., 2003. Giant submarine canyons: Is size any clue to their importance in the rock record? Geol. Soc. Am. Spec. Pap. 370, 175–190.
Normark, W.R., Posamentier, H., Mutti, E., 1993. Turbidite systems: State of the art and future directions. Rev. Geophys. 31, 91–116.
O'Grady, D.B., Syvitski, J.P., Pratson, L.F., Sarg, J.F., 2000. Categorizing the morphologic variability of siliciclastic passive continental margins. Geology 28, 207–210.
Olabode, S.O., Adekoya, J.A., 2007. Seismic stratigraphy and development of Avon canyon in Benin basin, southwestern Nigeria. J. Afr. Earth Sci. 50, 286–304.
Patacci, M., Haughton, P.D.W., McCaffrey, W.D., 2015. Flow Behavior of Ponded Turbidity Currents. J. Sediment. Res. 85, 885–902.
Paull, C.K., Caress, D.W., Ussler III, W., Lundsten, E., Meiner-Johnson, M., 2011. High-resolution bathymetry of the axial channels within Monterey and Soquel submarine canyons offshore central California. Geosphere 7, 1077–1101.
Peres, W.E., 1993. Shelf-fed turbidite system model and its application to the Oligocene deposits of the Campos Basin. AAPG Bull. 77, 88–101.
Petters, S.W., 1984. An ancient submarine canyon in the Oligocene-Miocene of the western Niger Delta. Sedimentology 31, 805–810.
Petter, A.L., Steel, R.J., 2006. Hyperpycnal plume formation from riverine outflows with small sediment concentrations. Sedimentology 48, 465–478.
Peyton, L., 1998. Interpretation of incised valleys using new 3D seismic techniques: A case history using spectral decomposition and coherency. Lead. Edge 17, 1294–1298.
Pickering, K., Coleman, J., Cremer, M., Droz, L., Kohl, B., Normark, W., O'Connell, S., Stow, D., Meyer-Wright, A., 1986. A high sinuosity, laterally migrating submarine fan channel-levee- overbank: results from DSDP Leg 96 on the Mississippi Fan, Gulf of Mexico. Mar. Petrol. Geol. 3, 3-18.
Posamentier, H.W., Kolla, V., 2003. Seismic geomorphology and stratigraphy of depositional elements in deepwater settings. J. Sediment. Res. 73, 367–388.
Poulsen, C.J., Flemings, P.B., Robinson, R.A., Metzger, J.M., 1998. Three-dimensional stratigraphic evolution of the Miocene Baltimore Canyon region: Implications for eustatic interpretations and the systems tract model. GSA Bull 110, 1105–1122.

Prather, B.E., 2003. Controls on reservoir distribution, architecture, and stratigraphic trapping in slope settings. Mar. Petrol. 20, 529–545.
Prather, B.E., Pirmez, C., Sylvester, Z., Prather, D.S., 2012. Stratigraphic response to evolving geomorphology in a submarine Apron perched on the upper Niger delta slope. SEPM Spec. Pub. 99, 145–161.
Pratson, L.F., Ryan, W.B., Mountain, G.S., Twichell, D.C., 1994. Submarine canyon initiation by downslope-eroding sediment flows evidence in late Cenozoic strata on the New Jersey continental slope. GSA Bull 106, 395–412.
Restrepo-Correa, I.C., Ojeda, G.Y., 2010. Geologic controls on the morphology of La Aguja submarine canyon. J. South Am. Earth Sci. 29, 861–870.
Riboulot, V., Cattaneo, A., Berné, S., Schneider, R.R., Voisset, M., Imbert, P., Grimaud, S., 2012. Geometry and chronology of late Quaternary depositional sequences in the Eastern Niger Submarine Delta. Mar. Geol. 319–322, 1–20. https://doi.org/10.1016/j.margeo.2012.03.002.
Rouby, D., Nalpas, T., Jermannaud, P., Robin, C., Guillocheau, F., Raillard, S., 2011. Gravity-driven deformation controlled by the migration of the delta front: the Plio- Pleistocene of the Eastern Niger Delta. Tectonophysics 513, 54–67.
Richardson, S.E., Davies, R.J., Allen, M.B., Grant, S.F., 2011. The structure and evolution of mass transport deposits in Azerbaijan's South Caspian Basin. Basin Res. 23, 702–719.
Shepard, F.P., 1981. Submarine canyons: Multiple causes and long-time persistence. AAPG Bull. 65, 1062–1077.
Shipp, R.C., Weimer, P., Posamentier, H.W., 2011. Mass-Transport Deposits in Deepwater Settings: An Introduction. In: Shipp, R.C., Weimer, P., Posamentier, H.W. (Eds.), Mass-transport Deposits in Deepwater Settings, vol. 96. SEPM Spec. Pub., pp. 3–6
Short, K.C., Stauble, A.J., 1967. Outline the geology of the Niger Delta. AAPG Bull. 51, 761–779.
Steffens, G.S., Biegert, E.K., Sumner, H.S., Bird, D., 2003. Quantitative bathymetric analysis of selected deepwater siliciclastic margins: receiving basin configuration for deepwater fan systems. Mar. Petrol. Geol. 20, 547–561.
Taner, M.T., Schuelke, J.S., O'Doherty, R., Baysal, E., 1994. Seismic attributes revisited. In: SEG Technical Program Expanded Abstracts, pp. 1104–1106.
Tuttle, W.L.M., Brownfield, E.M., Charpentier, R.R., 1999. The Niger Delta Petroleum System. Chapter A: Tertiary Niger Delta (Akata-Agbada) Petroleum System, Niger Delta Province, Nigeria, Cameroon, and Equatorial Guinea, Africa. U.S. Geological Survey, Open-File Report, 99-50.
Twichell, D.C., Roberts, D.G., 1992. Morphology, distribution, and development of submarine canyons on the US Atlantic Continental Slope between Hudson and Baltimore. Geology 10, 408–412.
Webb, S.D., 1981. Geology and palaeontology of the love bone bed from the Late Miocene of Florida. Am. J. Sci. 281, 513–544.
Weber, K.J., Duakoru, E.M., 1975. Petroleum geological aspects of the Niger Delta. J. Min. Geol. 12, 9–32.
Whiteman, A.J., 1982. Nigeria: its Petroleum Geology, Resources and Potential, vols. 1–2. Graham and Trotter, London, p. 394.
Wiener, R.W., Mann, M.G., Angelich, M.T., Molyneux, J.B., 2010. Mobile shale in the Niger Delta: Characteristics, structure, and evolution. In: Wood, L. (Ed.), Shale Tectonics, vol. 93. AAPG Memoir, pp. 145–161.
Wu, S., Bally, A.W., 2000. Slope tectonics. Comparisons and contrasts of structural styles of salt and shale tectonics of the northern Gulf of Mexico with shale tectonics of offshore Nigeria in the Gulf of Guinea. In: Mohriak, W., Talwani, M. (Eds.), Atlantic Rifts and Continental Margins. American Geophysical Union, Washington, D.C., pp. 151–172
Zhou, W., Wang, Y., Gao, X., Zhu, W., Xu, Q., Xu, S., Cao, J., Wu, J., 2015. Architecture, evolution history and controlling factors of the Baiyun submarine canyon system from the middle Miocene to Quaternary in the Pearl River Mouth Basin, northern South China Sea. Mar. Petrol. Geol. 67, 389–407.
Zhou, L., Sun, Z., Tang, G., Xiao, D., Cai, Z., Wang, H., Su, J., Hua, S., Ge, W., Chen, C., 2020. Pliocene's hyperpycnal flow and sedimentary pattern in the D block of Rakhine Basin in Bengal. Petrol. Explor. Dev. 47, 318–330.